*Graphical Abstract

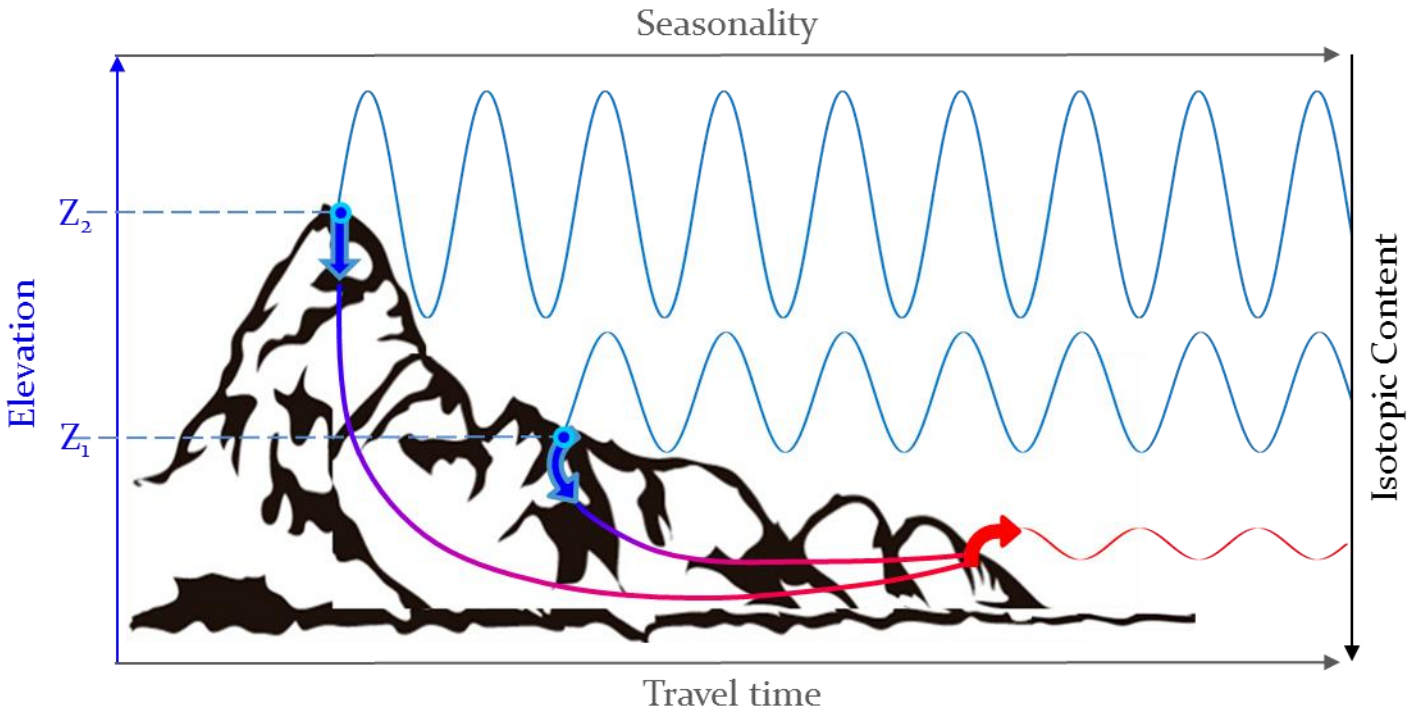

***Highlights (for review)**

Amplitude of seasonal isotopic composition of rainfall depends on elevation

Moisture generating rainfall at the PNOMP comes from a main source

The flow system tends to a better mixing the longer the system transit time is

The aquifer recharge zones located at elevations between 2600 and 1950 m a.s.l

Short transit times in agreement with the karstic nature of the aquifer system

Title

Vertical variation in the amplitude of the seasonal isotopic content of rainfall as a tool to jointly estimate the groundwater recharge zone and transit times in the Ordesa and Monte Perdido National Park aquifer system, north-eastern Spain.

Authors

Jorge Jódar Bermúdez, Groundwater Hydrology Group, Dept. Civil and Environmental Eng., Technical University of Catalonia (UPC) & Hydromodel Host S.L., Spain.

Emilio Custodio Gimena, Groundwater Hydrology Group, Dept. Civil and Environmental Eng., Technical University of Catalonia (UPC). Royal Academy of Sciences of Spain.

Luis Javier Lambán Jiménez, Geological Institute of Spain (IGME), Spain.

Sergio Martos Rosillo, Geological Institute of Spain (IGME), Spain.

Christian Herrera Lameli, Universidad Católica del Norte, Antofagasta, Chile.

Gonzalo Sapriza Azuri, Departamento del Agua, Centro Universitario Región Litoral Norte, Universidad de la República del Uruguay, Salto, Uruguay.

Corresponding author: J. Jódar, GHS, Department of Civil and Environmental Engineering, Technical University of Catalonia (UPC), Campus Nord- Building D2, C/ Jordi 14 Girona, 1-3, 08034, Barcelona. (jorge.jodar@hydromodelhost.com). Telf: +34 619712122.

Abstract

The time series of stable water isotope composition relative to meteorological stations and springs located in the high mountainous zone of the Ordesa and Monte Perdido National Park are analyzed in order to study how the seasonal isotopic content of precipitation propagates through the hydrogeological system in terms of the aquifer recharge zone elevation and transit time. The amplitude of the seasonal isotopic composition of precipitation and the mean isotopic content in rainfall vary along a vertical transect, with altitudinal slopes for $\delta^{18}O$ of 0.9 ‰/km for seasonal amplitude and -2.2 ‰/km for isotopic content. The main recharge zone elevation for the sampled springs is between 1950 and 2600 m.a.s.l. The water transit time for the sampled springs ranges from 1.1 to 4.5 yr, with an average value of 1.85 yr and a standard deviation of 0.8 yr. The hydrological system tends to behave as a mixing reservoir.

Keywords

Water isotopes, Seasonal isotopic amplitude, Transit time, Recharge, Alpine hydrology, Karst hydrology, Parque Nacional Ordesa y Monte Perdido

1. Introduction

In hydrological sciences, the stable water isotopes of precipitation have been widely used as natural tracers, taking advantage of the different processes affecting the atmospheric water vapor since it is generated until it produces precipitation (Gat, 1996; Mook and De Vries, 2000; Liotta et al., 2008). In most cases, these processes are affected by temperature-driven isotope fractionation (Dansgaard, 1964; Yurtsever and Gat, 1981; Rozanski et al., 1993; Araguás-Araguás et al., 2000; Mook and De Vries, 2000; Gonfiantini et al., 2001; Liebminger et al., 2006a; Stumpp et al., 2014, among others). The altitude effect (Mook, 2000; Rowley et al., 2001; Poage and Chamberlain, 2001; Liota et al., 2006; Fiorella, 2015 and references therein) and the seasonality effect (Gat, 1996; Mook and De Vries, 2000; Jódar et al., 2016) are the most relevant processes in mountainous zones.

The altitude effect refers to the empirical relationship between the isotopic content of rainfall (δ_{in}) and elevation (Z), which is described by the "altitudinal isotopic water line". This effect is generated by thermal air stratification enhanced by atmospheric advection, as the air masses climb up along the slopes of high mountains. The forced uplift generates an adiabatic expansion of the advected air parcels that cool them. This generates an orographic precipitation process in which vapor condensation increases (i.e. cloud droplets) and consequently precipitation is removed from the air parcel. In other words, the forced air uplift generates a Rayleigh cooling process (Gat, 1996) that fractionates the isotopic content of rainfall as the air parcel climbs up along the slopes of the mountain. As a result, the hydrogen and oxygen heavy isotope contents of precipitation decrease with increasing elevation (water becomes isotopically lighter). The isotopic lapse rate (i.e., depression of isotopic δ_{in} values per unit increase in elevation), even if steady in the long-term, is not stationary (Andreo et al., 2004; Liebminger et al., 2006b;

65 Fernández-Chacón et al., 2010; Kern et al., 2014). It may be affected by seasonal variations of
66 temperature because the altitude effect is a temperature-driven fractionation process.
67
68 The isotopic content of a water sample (m) is commonly given relative to a standard (s) and
69 expressed as $\delta = (R_m-R_s)/R_s$, where R is the ratio between the rare and the abundant isotope
70 concentrations, which for water refers to oxygen ($^{18}O/^{16}O$) and hydrogen ($^{2}H/^{1}H$). δ_{in} can be used
71 as a groundwater tracer in hydrological studies (Clark & Fritz, 1997; Gat, 1996; Kendall &
72 McDonnell, 1998; Lee & Krothe, 2001). Once the altitudinal isotopic water line has been locally
73 characterized, then the δ_{in} values can be used to identify the aquifer recharge areas and their
74 hydrogeological connection with the discharging springs (Lambán, 1998; Lambán and Custodio,
75 1999; Paternoster et al., 2008; Parisi 2011; Liota et al., 2013; Vallejos et al., 2015; among others)
76 if there is a well-defined recharge zone. Otherwise, when recharge is distributed over a wide
77 range of altitudes, there is a slope effect (Custodio, 2010; Custodio and Jódar, 2016). In this case,
78 the deduced altitude has not an easy meaning as it does not necessarily coincide with a centroid,
79 as flow pattern geometry and recharge distribution affect results.
80
81 The seasonality effect refers to the periodic oscillations of the isotopic composition of
82 precipitation generated by the seasonal changes of temperature. The seasonal isotopic content in
83 infiltrating precipitation enters as an input tracer signal in the hydrogeological system along with
84 recharge. This signal is buffered and delayed with respect to the input tracer signal as it
85 propagates through the hydrogeologic system. The differences between the input and the output
86 tracer signals (i.e. amplitude dampening and time shift) at the outlet of the system allow the
87 estimation of both the system transit time (τ) and the system transit time distribution (McGuire et
88 al., 2002; Reddy et al., 2006; Kabeya et al., 2007; Stumpp et al., 2009; Niinikoski et al. 2016;
89 among others). The transit time distribution provides a primary description of the hydrological

system behavior. It is usually inferred using lumped parameter models (LPM) (Małoszewski and Zuber, 1982; Amin and Campana, 1996; Leibundgut et al., 2011; Jódar et al., 2014). As LPMs do not require detailed hydrological knowledge of the physical system, they are especially well suited to study hydrological systems in karst and complex fractured zones, especially in mountainous areas where an internal detailed description of the most relevant hydrological features is often not available.

In mountainous zones, the altitude and seasonality effects are closely related given by their common dependence on temperature. The topographic altitudinal differences generate a vertical temperature gradient $\nabla_Z T$ that allows the Rayleigh cooling process to fingerprint the average altitudinal isotopic water line $\overline{\delta_{in}}(Z)$, which is usually assumed as stationary for average values. The seasonal variation of temperatures induces a seasonal variation in the isotopic content of rainfall along the vertical transect in which $\overline{\delta_{in}}(Z)$ exists. As a result of seasonality, the temporal dependence of the isotopic content of rainfall for a given elevation Z_i can be expressed as a sinusoidal function, with amplitude A_{in} and a mean value that coincides with $\overline{\delta_{in}}(Z_i)$. The spatial invariance of A_{in} is implicitly assumed in the numerous studies available in the bibliography. Given that τ is obtained as a function of the amplitude dampening at the outlet of the hydrogeological system (Małoszewski et al., 1982; McGuire and McDonnell, 2006), the assumption of a constant A_{in} allows the estimation of the hydrogeological system transit time τ without previously characterising $\overline{\delta_{in}}(Z)$. Nevertheless, in mountainous zones, A_{in} may depend on elevation (Jódar et al., 2016). The resulting vertical gradient of A_{in} (i.e. $\nabla_z A_{in}$) makes the τ estimation to be dependent of the previous characterization of $\overline{\delta_{in}}(Z)$. The hydrological implications of $\nabla_z A_{in}$ have not been addressed yet.

The objective of this work is twofold: 1) to present a methodological approach to account for $\nabla_z A_{in}$ in the jointly estimation of $\overline{\delta_{in}}(Z)$ and τ, and 2) to apply the methodology to the high-altitude karst aquifer system of Ordesa and Monte Perdido National Park (PNOMP), Spain. This is in order to explain the relationship between meteoric water recharge and the groundwater system in terms of the altitude of recharge and the transit time associated to the sampled springs. This will advance the fundamental understanding of the governing hydrological processes in the aquifer system of the PNOMP.

2. The study area

The PNOMP is located in the central sector of the Pyrenees (Fig. 1), which is the most important mountain chain of the Iberian Peninsula. The maximum altitude in the PNOMP corresponds to the Monte Perdido peak, 3355 m.a.s.l. (above sea level), the third highest peak of the entire Pyrenean range. The lowest point, at 689 m.a.s.l., is in Fuen dero Baño spring (site 22, Fig.1, Table 1).

From a climatic point of view, according to the Köppen-Geiger classification (Peel et al. 2007), the PNOMP has a cold climate with a dry season, with mild and cool summers and significant altitudinal variations. At the Fanlo-Góriz meteorological station (P1, Table 1), which is located at 2200 m.a.s.l., the mean annual temperature is 4.9 °C and the average precipitation is 1650 mm/yr. The average monthly precipitation presents a maximum of 220 mm in autumn, with a secondary peak of 185 mm in spring, and a minimum of 80 mm in winter. Rainfall spatial variability commonly shows a west to east gradient (Benito Alonso 2006) owing to the oceanic low pressure fronts arriving from the Atlantic. They are responsible for the main precipitation

volumes registered in the PNOMP (Lambán et al., 2015). In the study zone, the mean vertical gradients of precipitation and temperature are 200 mm/km and -3.3°C/km, respectively. The mean chloride content in precipitation is 0.87 mg/L, which is inside the range of 0.8 to 1.3 mg/L estimated by Alcalá and Custodio (2015) for this zone of the Pyrenees.

<Figure 1>

<Table 1>

From a geological point of view, the PNOMP has an alpine mountain landscape resulting mainly from a heterogeneous karstified land with numerous karren fields, caves, sinkholes and fissures, and from glacial processes. This is reflected in the long and deep U-shaped glacial valleys of Ordesa, Añisclo, Escuaín and Pineta. The PNOMP is part of the southern Pyrenean fold and thrust belt, which is formed by a set of imbricated thrust sheets (e.g., Seguret, 1972). The structural architecture of the PNOMP responds mainly to the two major thrust sheets, the Gavarnie basement thrust sheet and the Monte Perdido cover thrust sheet (Fig. 2). The Gavarnie thrust appears at the northern part of the study area, where Paleozoic and upper Cretaceous rocks crop out (Fig. 2), whereas the Monte Perdido thrust sheet comprises Cretaceous to lower Eocene rocks with subhorizontal bedding around the Ordesa Valley (Fig. 2). Towards the south, these rocks are highly tilted and overlain by middle Eocene turbidites. The upper Cretaceous and lower Paleocene-Eocene limestones, dolomites and calcarenites constitute the most important permeable outcropping materials and contain the most significant springs and water discharges. The main karst system is installed in the lower Paleocene-Eocene materials (CHE, 1998; Ríos-Aragüés, 2003; Lambán et al., 2015).

<Figure 2>

Groundwater in the PNOMP shows two principal hydrogeochemical facies (Fig.3): (A) calcium–bicarbonate or calcium–magnesium–bicarbonate composition in the 98% of the sampled springs, and (B) calcium–sulfate composition in some springs. These facies are in agreement with the carbonate nature of the main permeable materials found in the PNOMP: upper Cretaceous and lower Paleocene–Eocene limestones, dolomites and calcarenites. In the sampled springs, the average temperature T is 7.7 ºC and the electrical conductivity EC is 356 μS/cm. Based on groundwater (GW) tritium content, Lambán et al. (2015) inferred short residence times of water recharge through the aquifer, which is coherent with the conspicuous karst development in the PNOMP. The thermal spring of Fuen dero Baño (site 22) marks the exception in this general hydrogeochemical setting. This spring is located at the southernmost end of the PNOMP, relatively far away from the other sampled springs, at the lowest altitude sector (Fig. 1). Its water has an average T of 24°C and EC of 2980 μS/cm, and a sodium–chloride–sulfate composition (Fig 3).

<Figure 3>

Rainfall originating at the Atlantic Ocean is the main source of aquifer recharge in the PNOMP, as shown by the $\delta^{18}O$ and $\delta^{2}H$ seasonal averaged values (Fig. 4A). They plot very close to the Global Meteoric Water Line (GMWL) of 10 ‰ deuterium excess. In the case of the sampled springs (Fig. 4B), the isotopic composition of GW during autumn, winter and spring shows a greater average deuterium excess, close to 18‰. This is attributed to the daily cycle of diurnal snow sublimation and retained meltwater evaporation, and to the nocturnal condensation on the

187 snow pack covering the recharge area during that period (Stichler et al., 2001; Froehlich et al.,
188 2008; Christner et al., 2016).
189
190 The spring waters are isotopically more negative than the weighted long-term mean isotopic
191 composition of local rains (Fig. 4). This is attributed to a more or less constant seasonal recharge
192 coming from higher altitude recharge zones instead of a preferential recharge by winter rains.
193 Two facts support this assumption: (1) winter is the season that registers the lowest precipitation
194 in the PNOMP, and (2) snow covers the whole PNOMP area during autumn, winter and spring.
195
196 <Figure 4>
197
198 The isotopic water content sampled in the meteorological stations and springs of the PNOMP
199 show a seasonal dependence (Fig. 5). In the case of rainfall, the amplitude of the isotopic
200 seasonal variation increases with elevation. This effect has been also observed in meteorological
201 stations located along a vertical transect through the Alps (Jódar et al., 2016). In the case of GW,
202 the different amplitudes are related with the different transit time associated to each sampled
203 spring.
204
205 <Figure 5>
206
207
208 # 3. Methodology
209
210 ## 3.1 The conceptual model

The stable isotopes of water have become a useful tool to characterize the hydrological behavior of GW systems. Their use as tracers allows the estimation of the recharge zone elevation (Z_R) and the mean transit time (τ) of the hydrogeological systems by analyzing how the system transforms the input tracer function $\delta_{in}(t)$ into the measured output tracer function $\delta_{out}(t)$ at the outlet of the hydrological system (Małoszewski et al., 1983; Stewart and McDonnell, 1991; DeWalle et al., 1997; Kabeya et al., 2007, among others).

<Figure 6>

In classical hydrology, the estimation of τ has been approached as an independent process for the estimation of Z_R so far, because either the vertical variation of the input tracer amplitude A_{in} has not been considered as a tool for estimating transit times or A_{in} has been implicitly assumed as constant with elevation. If A_{in} and Z_R are considered independent variables, then the amplitude of the output tracer function depends only on the transit time of the hydrologic system, as shown in Jódar et al. (2014). In reference to this, for a given sinusoidal input tracer function with a fixed A_{in}, the analytical expression of the output tracer function in terms of the transit time is provided. Nevertheless, in mountainous zones with large altitudinal variations, A_{in} may depend on elevation, as shown by Jódar et al. (2016), for a vertical transect running through the Alps. They found a vertical gradient of $A_{\delta^{18}O}$ in rainfall (i.e. $\nabla_z A_{in}$) of 14.6‰/km. If A_{in} depends on elevation, then the dampening of the output tracer function and therefore the transit time estimation will depend on the recharge zone elevation Z_R as well.

3.2 Estimation of the dampening parameter

234 Let consider a hydrologic system response like that shown in Fig. 6. The amplitude decrease in
235 the output tracer function with/in respect to the input tracer function can be described by the
236 dampening factor, which is defined as

$$f = \frac{A_{out}}{A_{in}} \quad (1)$$

237

238 To estimate *f*, it is necessary to previously characterize both A_{in} and A_{out}.

239

240 The seasonal input and output tracer functions can be approached by using a sinusoidal function
241 (DeWalle et al., 1997; Kabeya et al., 2007; Jodar et al., 2016)

$$\delta_{in}(t) = A_\alpha \sin(\omega(t - t_0) + \varphi_\alpha) + \overline{\delta_\alpha} \quad (2)$$

242

243 where A is the amplitude of the tracer seasonal function, ω is the angular frequency, t is time, φ
244 is the angular shift for a reference time t_0, $\bar{\delta}$ is the mean tracer content, and the subscript α stands
245 for input and output, respectively.

246

247 Therefore, for a measured seasonal tracer function, it is possible to obtain the function
248 parameters A, φ and $\bar{\delta}$ in Eq. 2 that best fit the observed tracer measurements. This can be easily
249 done by using the solver of any of the commonly available spreadsheet software or manually.

250

251 3.3 Estimation of mean transit time

252 In complex and poorly characterized groundwater flow systems, Lumped Parameter Models
253 (LPMs) are often used to estimate τ. In particular, when $\delta_{in}(t)$ and $\delta_{out}(t)$ show seasonal patterns,

the Exponential-Piston model (EPM) and the Dispersion model (DM) (Małoszewski et al., 1982) LPMs are usually applied given that they allow the calculation of τ by using equation 3 for EPM and equation 4 for DM.

$$\tau_{EPM} = \frac{\eta}{\omega}\sqrt{\frac{1}{f^2} - 1} \tag{3}$$

$$\tau_{DM} = \frac{2}{\omega}\sqrt{\xi(1+\xi P_D)\left(\xi(1+\xi P_D) + \frac{1}{4P_D}\right)} \tag{4}$$

being ξ defined by convenience as

$$\xi = -\ln f \tag{5}$$

where f is the dampening factor, ω is the angular frequency of the tracer seasonal variation, η is the parameter of EPM and P_D is the parameter of DM.

To evaluate the aquifer mean transit time by taking profit of the output tracer dampening functions (Eq. 3 and 4), the transit time distribution that better describes the GW flow regime should be defined before. The most referenced transit time distributions are described in terms of the following LPM models: Piston flow model (PFM), Exponential model (EM), Exponential-Piston model (EPM) and Dispersion Model (DM). Although Małoszewski and Zuber (1982) provide schematic situations corresponding to the possible applicability of these models, a brief summary is given below.

(a) The lumped models PFM and DM can be used to simulate confined aquifers with a narrow recharge area located far from the groundwater sampling zone (Zuber, 1986).

(b) The EPM is the applicable lumped model in the case of an aquifer consisting of an unconfined upstream part and a confined downstream part (Zuber, 1986).

(c) In the case of unconfined aquifers with deep sampling points, the DM or the EPM should be used (Zuber, 1986).

(d) The EM can be applied to simulate the dynamics of groundwater systems in which the flow lines tend to converge towards the sampling points. This is especially true in the case of springs and shallow sampling points in unconfined aquifers (Dinçer and Davis, 1984; Eberts et al., 2012).

In the case of stable (non-radioactive) tracers, such as $\delta^{18}O$ and $\delta^{2}H$, the piston flow model does not modify the amplitude of the output tracer function. If this is the case, then f=1 and therefore τ cannot be estimated by using the dampening approach. If $f < 1$, transit time distributions other than PF can be considered. In this case, τ can be estimated by using Eq. 3 and 4 for EM and DM, respectively. In the case of EM, τ_{EM} can be directly obtained from Eq. 3 doing $\eta = 1$ (Amin and Campana, 1996).

To apply Eq. 3 and 4, it is necessary to previously know η and P_D. They are often adopted from bibliographic values obtained for aquifers with similar hydrogeological settings. As a result, the uncertainty of η or P_D is propagated into the τ estimation. Figure 7 shows how, for a tracer input

function with A_{in} =1 ‰, the output tracer amplitude A_{out} varies in terms of τ for different values of η and P_D, according to the model. As can be shown, for a given value of A_{out}, the larger the value of the LPM parameter the larger the obtained τ is.

<Figure 7>

The lumped-parameter approach transforms $\delta_{in}(t)$ into $\delta_{out}(t)$, according to Eq. 6, which is known as the convolution integral.

$$\delta_{out}(t) = \int_0^\infty \delta_{in}\,(t-t')g(t')dt' \tag{6}$$

where t is the time of entry, t' is the integration variable and $g(t')$ is the system response function specifying the transit time distribution of water through the system (Zuber, 1986).

For the case of a seasonal tracer input function (Eq.2), Jódar et al. (2014) provide the exact analytical solution of the convolution integral for different LPMs. In the case of EPM and DM, they are given by equations 7 and 8, respectively.

$$\delta_{out_{EPM}}(t) = \frac{\eta^2 A_{in}}{\eta^2+\omega^2\tau^2} sin\big(\omega\big(t-(t_0+t_\tau)\big)+\varphi_{in}\big) - \frac{\eta\omega\tau A_{in}}{\eta^2+\omega^2\tau^2} cos\big(\omega\big(t-(t_0+t_\tau)\big)+\varphi_{in}\big) + \overline{\delta_{in}} \tag{7}$$

$$\delta_{out_{EM}}(t) = A_{in} e^{\left(-u+\frac{1}{2P_D}\right)} sin(\omega(t-t_0)+\varphi_{in}-v) + \overline{\delta_{in}} \tag{8}$$

where the variables t_τ, u and v are defined by convenience as

$$t_\tau = \tau\left(1 - \frac{1}{\eta}\right) \quad (9)$$

$$u = 2\sqrt{\frac{1}{2P_D}}\sqrt{\sqrt{\omega^2\tau^2 + \left(\frac{1}{4P_D}\right)^2} + \frac{1}{4P_D}} \quad (10)$$

$$v = 2\sqrt{\frac{1}{2P_D}}\sqrt{\sqrt{\omega^2\tau^2 + \left(\frac{1}{4P_D}\right)^2} - \frac{1}{4P_D}} \quad (11)$$

As a result, for a given observed input and output seasonal tracer functions, it is possible to jointly estimate τ and the model parameter (i.e. η or P_D) by using equation 7 and 8, for EPM and DM, respectively. The procedure to do this is summarized as:

1. Calibration of the input function parameters (A_{in}, φ_{in} and $\overline{\delta_{in}}$) from Eq. 5 as explained in section 3.1.1.

2. Selection of the LPM (i.e. EPM or DM) according to the particular hydrogeological situation at hand (Małoszewski and Zuber 1982).

3. Calibration of the output function parameters from Eq. 7 or 8 (i.e., τ and η or $P_{D,}$ depending on the selected LPM) to fit the output tracer measurements. As in step 1, calibration can be performed either automatically or manually.

3.4 Estimation of aquifer recharge elevation

To estimate the elevation of well-defined aquifer recharge zones the approach can be summarized as follows:

1. Obtaining the Local Isotopic Altitudinal Line $Z(\bar{\delta})$ (Fig. 8A) as the linear regression between the elevation Z_{P_j} (j=1, Num. Met. Stations) of the different meteorological stations and their corresponding mean isotopic content in precipitation $\overline{\delta_{P_j}}$. The $\overline{\delta_{P_j}}$ values are obtained by applying the Sin-wave regression model described in section 3.1.1.

2. Obtaining the recharge elevation Z_R of the discharging spring. This is done by evaluating $Z(\bar{\delta})$ for an isotopic content equal to the mean isotopic water content in the spring $\overline{\delta_{out}}$ (Fig. 8B). By doing this, it is assumed that both the recharge and discharge zones are located in a specific zone along the vertical transect. Otherwise, the sloping tracer effect should be taken into account to estimate Z_R (Custodio and Jódar, 2016). $\overline{\delta_{out}}$ is obtained by applying the Sin-wave regression model described in section 3.1.1.

3. Obtaining the isotopic amplitude altitudinal line $A(Z)$ (Fig. 8C) as the linear regression between the amplitude of the seasonal isotopic water content in rainfall A_{P_j} (j=1, Num. Met. Stations) associated to the different meteorological stations and their corresponding elevation Z_{P_j}. The A_{P_j} values are obtained by applying the Sin-wave regression model described in section 3.1.1.

4. Obtaining the amplitude A_{Z_R} of the isotopic input function associated to the recharge elevation Z_R of the discharging spring by evaluating $A(Z)$ for an elevation equal to Z_R (Fig. 8D).

354 <Figure 8>

355

356

357 ## 4. Field work

358 Since July 2007, periodical GW sampling has been carried out in 13 of the most representative
359 springs of the PNOMP (Table 1 and Fig. 1), covering a wide range of elevations, with the aim of
360 studying the spatio-temporal chemical and isotopic GW content trends in the PNOMP. In all
361 cases, electrical conductivity (EC), pH and temperature (T) were measured in situ.

362

363 The isotope content in the water samples were analysed at the Stable Isotopes Laboratory of
364 CETA-CEDEX (2007), IACT-CSIC (2011-2012) and UAM (2013-2015). In the CETA-CEDEX
365 laboratory, $\delta^{18}O$ and $\delta^{2}H$ were measured by SMS (small mass spectrometer), a Delta Plus
366 Advantage model by Finnigan MAT. The isotopic composition of oxygen was determined
367 through the water–CO_2 equilibration technique and that of hydrogen, through the water–H_2
368 equilibration technique using a platinum catalyst. The reproducibility calculated from standards
369 systematically interspersed in the analytical batches is ±0.2 ‰ for $\delta^{18}O$ and ± 1.5‰ for $\delta^{2}H$. The
370 laboratory standards were regularly calibrated according to international standards (Vienna
371 Standard Mean Ocean Water, VSMOW). In the IACT-CSIC (Granada), the $\delta^{18}O$ and $\delta^{2}H$ were
372 analyzed with a Finnigan Delta Plus XL mass spectrometer. The measurement errors for $\delta^{18}O$
373 and $\delta^{2}H$ are ±0.1 and ±1.5‰, respectively. In the UAM Laboratory, the $\delta^{18}O$ and $\delta^{2}H$ were
374 analyed by pyrolisis in an Elemental Analyzer Thermo 1112 HT Flash coupled to an IRMS
375 Thermo Delta V Advantage (Bremen, Germany).The measurement errors for $\delta^{18}O$ and $\delta^{2}H$ are ±
376 0.1 and ±1‰, respectively. All results are given relative to the V-SMOW standard.

377

Monthly bulked samples of rainfall have been taken along with the GW sampling campaign at the meteorological stations of Parador and Góriz (Table 1 and Fig. 1). The rain gauges consist on a 40-cm diameter low-density polyethylene (LDPE) funnel that captures and guides precipitation into a 5 L LDPE bottle, where about 350 mL of Vaseline oil is added to avoid evaporation. To protect the bottle with the water sample from direct sunlight, it was set into a 30L LDPE container.

The meteorological station of Fiscal (Fig. 1) is located in the village of Borrastre-Fiscal, at 735 m.a.s.l. It provided valuable information regarding the isotopic content of rainfall at the low elevation surroundings of PNOMP. The isotopic data correspond to rainfall samples of single rainfall episodes collected from May 2011 to August 2013 (Moreno et al., 2015). The monthly weighted mean isotopic value for the *i*-th month is calculated as

$$\delta_i = \frac{\sum_{j=1}^{N_i} P_j \delta_j}{\sum_{j=1}^{N_i} P_j} \quad (12)$$

where δ_i is the monthly averaged isotopic content of the rainfall, N_i is the number of rainfall episodes and δ_j and P_j are respectively the isotopic content of the rainfall and the precipitation volume corresponding to the *j*-th rainfall episode.

5 Results and Discussion

The seasonal isotopic time series measured in all the meteorological stations and springs are fitted by calibrating the parameters A, φ and $\bar{\delta}$ of Eq. 2 (Tables 2 and 3). Fig. 5 shows the

observed and the fitted isotope content in rainfall and GW for all the sampled sites (i.e. meteorological stations and springs).

In the case of rainfall, both the mean isotopic content (i.e. $\overline{\delta^{18}O}_{in}$) and the seasonal isotopic amplitude (i.e. $A_{\delta^{18}O_{in}}$) show a linear relationship with elevation (Fig 8). The respective coefficients of determination are 0.99 and 0.87. Generally, the more elevated the meteorological station is (1) the more negative the mean isotopic content and (2) the larger the seasonal isotopic amplitude is. The vertical gradient of the mean isotopic content in precipitation $\nabla_Z\overline{\delta^{18}O}_{in}$ is -2.2 ‰/km, which is coherent with the gradient values obtained for different alpine mountainous zones (Poage and Chamberlain, 2001). The vertical gradient of the seasonal isotopic amplitude $\nabla_Z A_{\delta^{18}O_{in}}$ is 0.9 ‰/km, which is close to that obtained by Jódar et al. (2016) for a vertical transect running through the Alps. Moreover, the fact of having an increasingly monotonic relationship between $A_{\delta^{18}O_{in}}$and elevation points towards the existence of a major common source of moisture for the three sampled meteorological stations in the PNOMP (Jódar et al., 2016). This result confirms the findings of Lambán et al. (2015) in this regard, who found that precipitation in the PNOMP mostly comes from the Atlantic. This result was based on the empirical relationship between precipitation events in the PNOMP and their corresponding synoptic general atmospheric circulation pattern (Goodess and Palutikof, 1998; Cortesi et al., 2013; Sapriza-Azuri et al., 2013, 2015; Gupta et al. 2016).

<Table 2>

<Figure 9>

The mean isotopic content in GW (i.e. $\overline{\delta^{18}O}_{out}$) for the springs varies between -12.2 ‰ (site 9) and -9.6 ‰ (site 22) (Table 3), showing a mean vertical gradient (i.e. $\nabla_z\overline{\delta^{18}O}_{out}$) of -1.3 ‰/km. This vertical gradient is similar to that reported by Arce et al. (2001) and Iribar and Antigüedad (1996) for the western Pyrenees. $\nabla_z\overline{\delta^{18}O}_{out}$ is smaller than that obtained for precipitation (Fig. 8A), indicating that GW sampled in the springs comes from a well-mixed reservoir (Custodio and Jódar, 2016). The amplitude of the seasonal isotopic content in GW (i.e. $A_{\delta^{18}O_{out}}$) ranges from 0.19 ‰ (site 10) to 2.78 ‰ (site 18) and the corresponding vertical gradient of the seasonal isotopic amplitude (i,e, $\nabla_Z A_{\delta^{18}O_{out}}$) is 1.6 ‰/km, larger than that obtained for rainfall.

The estimated transit time ranges from 1.12 yr (site 18) to 4.48 yr (site 6A), with an average value of 1.85 yr and a standard deviation of 0.8 yr. This result confirms the short transit times of recharge water through the aquifer obtained by Lambán et al. (2015) for some springs by analyzing the tritium content in GW. In fact, the obtained spatial distribution of transit times is coherent with their hydrogeological conceptual model. The springs with the shortest transit time (i.e. sites 18, 19, 23 and 9) correspond to those springs discharging GW from the Eocene-Paleocene materials. The springs with the longest transit time (i.e. sites 6A, 6B, 4, 42, 43 and 44) correspond to springs discharging GW from the Upper Cretaceous materials.

The aquifer is assumed to behave as an EPM system, which consists of two parts in line, one with Piston Flow (PF) distribution of transit times and another with Exponential (EM) distribution of transit times. The PF part only delays while the EM delays and buffers the input tracer signal (Małoszewski and Zuber, 1982). Figure 10A shows the obtained dependence between *f* and τ for the sampled springs. The larger the τ value the smaller the dampening factor *f* is.

The EPM is characterized by the lumped parameter η, which is defined as the ratio of the total system volume to the volume with the exponential distribution of transit times. The values of η range from 1 (i.e. exponential flow model) to infinite. Therefore, $1/\eta$ ranges from 0 to 1. Figure 10B shows the relationship obtained between $1/\eta$ and τ for the sampled springs. The volume associated to the EM distribution of transit times increases as the hydrologic system transit time increases, and conversely. This result shows how the system integrates the contribution of the different flow lines in the aquifer discharge. The springs discharging GW of short length flow lines correspond to springs having a greater proportion of PF distribution of transit times in sampled GW, therefore with a low dampening effect respect to the input tracer function. As the transit time increases, the length of the aquifer flow lines increases accordingly. This favors the transition towards a perfect mixing (i.e. EM) distribution of transit times, vanishing the role played by the PF part in the hydrological system response.

<Table 3>

<Figure 10>

The estimated Z_R values for the sampled springs are mostly comprised between $Z_{R_{Max}}$= 1950 m (i.e. site 6B) and $Z_{R_{Min}}$= 2632 m.a.s.l. (i.e. site 9), within an elevation range of 682 m. This result is coherent with that obtained by Polo (2015), who applied a modified APLIS method (Andreo et al., 2008) to map the spatial distribution of recharge zones in the PNOMP. Figure 11A shows the spatial distribution of the Rainfall Infiltration Capacity (RIC) at the PNOMP. Figure 11-B shows the corresponding variation of RIC along elevation. RIC ranges from 40 to 60%, showing a

slight increase with elevation which is conditioned by both the more intense karst development and the reduction of vegetation with elevation.

To facilitate the use of the vertical variation of A_{in} with elevation as a hydrological characterization tool in other zones, it is worth noting that recharge is assumed to be constant along the year in the PNOMP. This assumption explains why the observed isotopic content of GW is isotopically more negative than the weighted long-term mean isotopic composition of local rains (Fig. 4). Nevertheless, if recharge shows a clear seasonal pattern $R(t)$, with preferential recharge by winter rains, the effect on the isotopic content of GW would be the same as the observed in the PNOMP (i.e. a lower isotopic content of GW with respect to the long-term mean isotopic composition of local rains). If this was the case, the effect of a seasonal recharge $R(t)$ would be translated to the output tracer function as a lower mean isotopic content in the spring water. By applying the methodology described in Fig. 4 to this lower mean isotopic content, a higher elevation recharge will be obtained and hence a larger input isotopic amplitude. This will produce a smaller dampening factor f than in turn will result in estimating a larger transit time.

The vertical variation of A_{in} with elevation can be used to obtain more information on the hydrological system than just the elevation of the recharge zone and the associated transit time. It can be used to investigate other hydrological processes controlling the behavior of the hydrological system. In this line, if one takes into account (1) the moderate to high rainfall infiltration capacity existing in almost the whole study area, (2) the transit time increase along the GW flow line, and (3) the evolution towards a EM as the hydrologic system transit time increases (Fig.9B), one would expect to have the longest τ and the smallest A_{out} for the sampled

spring with the lowest elevation (i.e. site 22). That does not definitively happen. A likely hypothesis for explaining this unexpected behavior is considering the GW samples from site 22 (Fig.3) to be a mix of two different GW sources (Lambán et al., 2015): (1) GW_1 coming from local recharge with a relatively short transit time, showing the seasonal variation of the input tracer function, and (2) GW_2 as the discharge from a regional aquifer with a long transit time, saline input and damped out seasonal isotopic content. So, the isotopic content of GW samples from site 22 can be a linear combination of these two end members, expressed as:

$$\overline{\delta^{18}\mathrm{O}_{GW_{22}}} = (1-\chi)\cdot\overline{\delta^{18}\mathrm{O}_{GW_1}} + \chi\cdot\overline{\delta^{18}\mathrm{O}_{GW_2}} \quad (13)$$

$$\overline{\delta^{2}\mathrm{H}_{GW_{22}}} = (1-\chi)\cdot\overline{\delta^{2}\mathrm{H}_{GW_1}} + \chi\cdot\overline{\delta^{2}\mathrm{H}_{GW_2}} \quad (14)$$

$$\overline{\delta^{2}\mathrm{H}_{GW_2}} = 8\cdot\overline{\delta^{18}\mathrm{O}_{GW_2}} - 10 \quad (15)$$

where $\overline{\delta^{18}\mathrm{O}_{GW_{22}}}$ and $\overline{\delta^{2}\mathrm{H}_{GW_{22}}}$ are the mean isotopic content in GW for site 22. The first one is -9.60 ‰ (Table 3) and the second one is obtained by applying the Sin-wave regression model described in section 3.1.1 to the deuterium time series measured in Site 22, obtaining $\overline{\delta^{2}\mathrm{H}_{GW_{22}}}$ = -67.73 ‰ (Table 4). The variables $\overline{\delta^{18}\mathrm{O}_{GW_1}}$ and $\overline{\delta^{2}\mathrm{H}_{GW_1}}$are the mean isotopic content of GW_1. As the mean seasonal content of a stable conservative tracer is not affected by the system transit time (Jódar et al., 2014), the values for $\overline{\delta^{18}\mathrm{O}_{GW_1}}$ and $\overline{\delta^{2}\mathrm{H}_{GW_1}}$ coincide with those of rainfall at the corresponding recharge elevation Z_R. As Z_R for site 22 is unknown, it is assumed that it is between $Z_{R_{Max}}$ (i.e Z_R of site 9) and $Z_{R_{Min}}$ (i.e Z_R of site 6B), which is the elevation interval comprising all the other sampled springs (Table 3). The mean isotopic content in rainfall for $Z_{R_{Max}}$ and $Z_{R_{Min}}$ coincides with that of site 9 and site 6B, respectively (Table 3). In both cases, $\overline{\delta^{2}\mathrm{H}_{GW_1}}$ is obtained by applying the Sin-wave regression model described in section 3.1.1 to the

deuterium time series measured in site 9 and site 6B to obtain $Z_{R_{Max}}$ and $Z_{R_{Min}}$, respectively (Table 4). The unknown variables in the equation system are the GW mixing proportion χ [-] and the mean isotopic content of GW_2 given by $\overline{\delta^{18}O_{GW_2}}$ and $\overline{\delta^{2}H_{GW_2}}$. These two variables are assumed to be not independent and related by the global mean meteoric water line, which is described by Equation 15. The analytical solution to the above equation system is given by

$$\chi = \frac{8 \cdot \left(\overline{\delta^{18}O_{GW_1}} - \overline{\delta^{18}O_{GW_{22}}}\right) + \overline{\delta^{2}H_{GW_{22}}} - \overline{\delta^{2}H_{GW_1}}}{8 \cdot \overline{\delta^{18}O_{GW_1}} - \overline{\delta^{2}H_{GW_1}} - 10} \quad (16)$$

$$\overline{\delta^{18}O_{GW_2}} = \frac{\overline{\delta^{18}O_{GW_1}} \cdot \left(10 + \overline{\delta^{2}H_{GW_{22}}}\right) - \overline{\delta^{18}O_{GW_{22}}} \cdot \left(10 + \overline{\delta^{2}H_{GW_1}}\right)}{8 \cdot \left(\overline{\delta^{18}O_{GW_1}} - \overline{\delta^{18}O_{GW_{22}}}\right) + \overline{\delta^{2}H_{GW_{22}}} - \overline{\delta^{2}H_{GW_1}}} \quad (17)$$

The different mixing proportions of GW1 and GW2 that explain the observed mean isotopic content in the groundwater discharging in site 22 in terms of Z_R are given in Table 4. The proportion of GW_2 discharging in site 22 linearly decreases from 39% to 28% for Z_R increasing from $Z_{R_{Min}}$ to $Z_{R_{Max}}$.

<Table 4>

Under the hypothesis that chloride behaves as a conservative tracer and that chloride concentration in recharge water (i.e. WG_1) is the same than that of rainfall (i.e. 0.87 mg/L), and knowing the chloride concentration of GW_{22} (i.e. 658 mg/L), it is possible to estimate the chloride content of WG_2 by taking into account the GW mixing proportions defined by χ (Table 4). As a result, the chloride concentration in the regional discharge WG_2 increases from 1686 to 2348 mg/L for Z_R increasing from $Z_{R_{Min}}$ to $Z_{R_{Max}}$. These chloride concentrations are coherent with those measured by CHE (2004) in the springs of Tiermas (2709-1-0002), Olza (2508-1-

0004) and Sotonera (2911-1-0010/2911-1-0012) that discharge GW from Upper Cretaceous-Paleocene-Eocene materials in the neighbouring of the PNOMP.

<Table 5>

5 Conclusions

In the southern side of the central Pyrenees mountain range there is a linear relationship between the amplitude of the seasonal isotopic content of rainfall A_{in} and elevation. This increasingly monotonic relationship confirms the Atlantic Ocean as the major source of moisture for precipitation in the PNOMP, as suggested by other authors.

The recharge zone for the sampled springs is located at an elevation ranging from 2600 and 1950 m.a.s.l. As the isotopic signal of rainfall propagates through the hydrologic system as recharge, the existence of a vertical gradient in the amplitude of the seasonal isotopic content of rainfall $\nabla_Z A_{in}$ has a direct effect on the system response. Therefore, it must be accounted when the system transit time is obtained as a dampening function of the seasonal isotopic output function.

The hydrogeological system presents short transit times, in agreement with the karstic nature of the aquifer system. Despite the small dispersion of transit time values obtained for the sampled springs, its distribution points to better mixing the longer the system transit time is.

GW discharging through the thermal spring of Fuen dero Baño can be explained as the result of a mixing between two components: one coming from local recharge with a relatively short transit time and between 28% and 39% of total discharge coming from a regional flow system.

Acknowledgements

This research was undertaken in the framework of the CANOA-73.3.00.44.00 project ‘‘Hydrological behavior analysis of groundwater dependent wetlands’’, funded by the Geological Institute of Spain (IGME), and the “Anillo Project” ACT-1203 of the CONICYT, Chile. The authors would like to thank the Ordesa and Monte Perdido National Park Direction (Gobierno de Aragón), Elena Villagrasa from DGA, Fernando Carmena and Ignacio Gómez from SARGA, the Góriz Mountain Hut Wardens and especially Ana Moreno and Blas Valero from the Pyrenean Institute of Ecology (IPE-CSIC) for their collaboration. Meteorological data have been provided by the Spanish Meteorological Agency (AEMET).

We would also like to thank the anonymous reviewers for their constructive comments and suggestions which led to a substantial improvement of the paper

References

Alcalá, F.J., Custodio, E. (2015). Natural uncertainty of spatial average aquifer recharge through atmospheric chloride mass balance in continental Spain. J. Hydrol., 524: 642-661. DOI:10.1016/j.jhydrol.2015.03.018.

579 Andreo, B., Linan, C., Carrasco, F., De Cisneros, C.J., Caballero, F., Mudry, J. (2004). Influence
580 of rainfall quantity on the isotopic composition (18O and 2H) of water in mountainous areas.
581 Application for groundwater research in the Yunquera-Nieves karst aquifers (S Spain). Applied
582 Geochemistry, 19(4): 561-574. DOI:10.1016/j.apgeochem.2003.08.002.
583
584 Amin, I.E., Campana, M.E. (1996). A general lumped parameter model for the interpretation of
585 tracer data and transit time calculation in hydrologic systems. J. Hydrol., 179(1): 1-21.
586 DOI:10.1016/0022-1694(95)02880-3.
587
588 Andreo, B.; Vías, J.M.; Durán, J.J.; Jiménez, P.; López Geta, J.A., Carrasco, F. (2008).
589 Methodology for groundwater recharge assessment in carbonate aquifers: application to pilot
590 sites in southern Spain. Hydrogeol. J. 16: 911-925. DOI:10.1007/s10040-008-0274-5.
591
592 Araguás-Araguás, L., Froehlich, K., and Rozanski, K. (2000). Deuterium and oxygen-18 isotope
593 composition of precipitation and atmospheric moisture. Hydrol. Processes, 14(8): 1341-1355.
594 DOI:10.1002/1099-1085(20000615)14:8<1341::AID-HYP983>3.0.CO;2-Z.
595
596 Arce M, García MA, Arqued V. (2001). Caracterización del oxígeno 18, deuterio y tritio en las
597 aguas del Pirineo. In: Las Caras del Agua Subterránea. Serie: Hidrogeología y Aguas
598 Subterráneas. IGME, Madrid: 387-393.
599
600 Benito Alonso, J.L. (2006). Vegetación del Parque Nacional de Ordesa y Monte Perdido. Serie
601 Investigación 50. Consejo de Protección de la Naturaleza de Aragón. Zaragoza.
602

603 CHE (1998). Catalogación de los acuíferos de la Cuenca del Ebro. Oficina de Planificación
604 Hidrológica. Confederación Hidrográfica del Ebro, Zaragoza.
605
606 CHE (2004). Caracterización hidroquímica de las aguas subterráneas del Dominio Sinclinal de
607 Jaca – Pamplona.
608
609 Clark, I., Fritz, P. (1997). Environmental isotopes in hydrogeology. Lewis Publishers, New
610 York: 1-328.
611
612 Cortesi, N., Trigo, R.M., Gonzalez-Hidalgo, J.C., Ramos, A.M. (2013). Modelling monthly
613 precipitation with circulation weather types for a dense network of stations over Iberia.
614 Hydrology and Earth System Sciences, 17(2): 665-678. DOI:10.5194/hess-17-665-2013.
615
616 Christner, E., Kohler, M., Schneider, M. (2016). The influence of snow sublimation on stable
617 isotopes of water vapor in the atmospheric boundary layer of Central Europe. Atmos. Chem.
618 Phys. Discuss., DOI:10.5194/acp-2016-461.
619
620 Custodio, E. (2010). Estimation of aquifer recharge by means of atmospheric chloride deposition
621 balance in the soil. Contributions to Science, 6(1): 81–97. DOI:10.2436/20.7010.01.86.
622
623 Custodio, E., Jódar, J. (2016). Simple solutions for steady–state diffuse recharge evaluation in
624 sloping homogeneous unconfined aquifers by means of atmospheric tracers. J. Hydrol.
625 DOI:10.1016/j.jhydrol.2016.06.035.
626

627 Dansgaard, W. (1964). Stable isotopes in precipitation. Tellus, 16(4): 436-468.
628 DOI:10.1111/j.2153-3490.1964.tb00181.x.
629
630 DeWalle, D.R., Edwards, P.J., Swistock, B.R., Aravena, R., Drimmie, R.J. (1997). Seasonal
631 isotope hydrology of three Appalachian forest catchments. Hydrol. Processes, 11(15): 1895-
632 1906. DOI:10.1002/(SICI)1099-1085(199712)11:15<1895::AID-HYP538>3.0.CO;2-%23.
633
634 Dinçer, T., Davis, G.H., 1984. Application of environmental isotope tracers to modeling in
635 hydrology. J. Hydrol. 68 (1), 95–113.
636
637 Eberts, S.M., Böhlke, J.K., Kauffman, L.J., Jurgens, B.C., 2012. Comparison of particletracking
638 and lumped-parameter age-distribution models for evaluating vulnerability of production wells
639 to contamination. Hydrogeol. J. 20 (2), 263–282, 10.1007/s10040-011-0810-6.
640
641 Fernández-Chacón, F., Benavente, J., Rubio-Campos, J. C., Kohfahl, C., Jiménez, J., Meyer, H.,
642 Hubberten, H., Pekdeger, A. (2010), Isotopic composition ($\delta^{18}O$ and δD) of precipitation and
643 groundwater in a semi-arid, mountainous area (Guadiana Menor basin, Southeast Spain). Hydrol.
644 Processes, 24: 1343–1356. DOI:10.1002/hyp.7597.
645
646 Fiorella, R.P., Poulsen, C.J., Pillco Zolá, R.S., Barnes, J.B., Tabor, C.R., Ehlers, T.A. (2015).
647 Spatiotemporal variability of modern precipitation $\delta^{18}O$ in the central Andes and implications for
648 paleoclimate and paleoaltimetry estimates. J.Geophys. Res.: Atmospheres, 120(10): 4630-4656.
649 DOI:10.1002/2014JD022893.
650

651 Froehlich, K., Kralik, M., Papesch, W., Rank, D., Scheifinger, H., Stichler, W. (2008).
652 Deuterium excess in precipitation of Alpine regions — moisture recycling. Isotopes in
653 Environmental and Health Studies, 44(1): 1–10. http://dx.doi.org/10.1080/10256010801887208.
654
655 Gat, J.R. (1996). Oxygen and hydrogen isotopes in the hydrologic cycle. Annual Review of
656 Earth and Planetary Sciences, 24(1): 225-262. DOI:10.1146/annurev.earth.24.1.225.
657
658 Gonfiantini, R., Roche, M.A., Olivry, J.C., Fontes, J.C., Zuppi, G.M. (2001). The altitude effect
659 on the isotopic composition of tropical rains. Chem. Geol., 181(1): 147-167.
660 DOI:10.1016/S0009-2541(01)00279-0.
661
662 Goodess, C.M., Palutikof, J.P. (1998). Development of daily rainfall scenarios for southeast
663 Spain using a circulation-type approach to downscaling. Inter. J. Climatol., 18: 1051–1083.
664 DOI:10.1002/(SICI)1097-0088(199808)18:10<1051::AID-JOC304>3.0.CO;2-1.
665
666 Gupta, H.V., Sapriza-Azuri, G., Jódar, J., Carrera, J. (2016). Circulation pattern-based
667 assessment of projected climate change for a catchment in Spain. J. Hydrol.
668 DOI:10.1016/j.jhydrol.2016.06.032.
669
670 IGME-OAPN (2013). Guía geológica del Parque Nacional de Ordesa y Monte Perdido. Guías
671 Geológicas de Parques Nacionales. Instituto Geológico y Minero de España- Organismo
672 Autónomo de Parques Nacionales, Madrid. Editorial Everest: 1-214.
673

Iribar, V., Antigüedad, I. (1996). Definición de zonas de recarga de manantiales kársticos mediante técnicas isotópicas ambientales. In: Simp. Rec. Hidr. en Regiones Kársticas, Vitoria-Gasteiz. Gob. Vasco/AIH-GE: 271–280.

Jódar, J., Lambán. L.J., Medina, A., Custodio, E. (2014). Exact analytical solution of the convolution integral for classical hydrogeological lumped-parameter models and typical input tracer functions in natural gradient systems. J. Hydrol., 519: 3275–3289. DOI:10.1016/j.jhydrol.2014.10.027.

Jódar, J., Custodio, E., Liotta, M., Lambán, L.J., Herrera, C., Martos-Rosillo, S., Sapriza, G., Rigo, T. (2016). Correlation of the seasonal isotopic amplitude of precipitation with annual evaporation and altitude in alpine regions. Sci. Total Environ., 550: 27-37. DOI:10.1016/j.scitotenv.2015.12.034.

Kabeya, N., Katsuyama, M., Kawasaki, M., Ohte, N., Sugimoto, A. (2007). Estimation of mean residence times of subsurface waters using seasonal variation in deuterium excess in a small headwater catchment in Japan. Hydrol. Processes, 21(3): 308-322. DOI:10.1002/hyp.6231.

Kendall, C., McDonnell, J.J. (1998). Isotope tracers in catchment hydrology. Elsevier, Amsterdam.

Kern, Z., Kohán, B., Leuenberger, M. (2014). Precipitation isoscape of high reliefs: interpolation scheme designed and tested for monthly resolved precipitation oxygen isotope records of an Alpine domain. Atmospheric Chemistry and Physics, 14(4): 1897-1907. DOI:10.5194/acp-14-1897-2014.

Lambán, L.J. (1998). Estudio de la recarga y del funcionamiento hidrogeológico de la Unidad Anoia (Cordillera Prelitoral Catalana). Ph.D. Thesis. Technical University of Catalonia.

Lambán, L.J.; Custodio, E. (1999). Estudio isotópico ambiental (O^{18}–D) en la unidad Anoia: principales zonas de recarga e implicaciones en el funcionamiento hidrogeológico del sistema. Ingeniería del Agua, 6(2): 139–150.

Lambán, L.J., Jódar, J., Custodio, E., Soler, A., Sapriza, G., Soto, R. (2015). Isotopic and hydrogeochemical characterization of high-altitude karst aquifers in complex geological settings. The Ordesa and Monte Perdido National Park (Northern Spain) case study. Sci. Total Environ., 506: 466-479. DOI:10.1016/j.scitotenv.2014.11.030.

Lee, E.S., Krothe, N.C. (2001). A four-component mixing model for water in karst terrain in south-central Indiana, USA, using solute concentration and stable isotopes as tracers. Chem. Geol. 179: 129–143. DOI:10.1016/S0009-2541(01)00319-9.

Leibundgut, C., Małoszewski, P., Külls, C., (2011). Tracers in hydrology. John Wiley & Sons.

Liebminger, A., Haberhauer, G., Papesch, W., Heiss, G., (2006a). Correlation of the isotopic composition in precipitation with local conditions in alpine regions. J. of Geophys. Res.: Atmospheres, 111(D5). DOI:10.1029/2005JD006258.

722 Liebminger, A., Haberhauer, G., Varmuza, K., Papesch, W., Heiss, G. (2006b). Modeling the
723 oxygen 18 concentration in precipitation with ambient climatic and geographic parameters.
724 Geophysical Research Letters, 33(5). DOI:10.1029/2005GL025049.
725
726 Liotta, M., Favara, R., Valenza, M. (2006). Isotopic composition of the precipitations in the
727 central Mediterranean: Origin marks and orographic precipitation effects. Journal of Geophysical
728 Research: Atmospheres, 111(D19). DOI:10.1029/2005JD006818.
729
730 Liotta, M., Bellissimo, S., Favara, R., Valenza, M. (2008). Isotopic composition of single rain
731 events in the central Mediterranean. J. Geophys. Res.: Atmospheres, 113, D16304.
732 DOI:10.1029/2008JD009996.
733
734 Liotta, M., Grassa, F., D'Alessandro, W., Favara, R., Candela, E.G., Pisciotta, A., Scaletta, C.
735 (2013). Isotopic composition of precipitation and groundwater in Sicily, Italy. Applied
736 Geochemistry, 34, 199-206. DOI:10.1016/j.apgeochem.2013.03.012.
737
738 Małoszewski, P., Zuber, A. (1982). Determining the turnover time of groundwater systems with
739 the aid of environmental tracers, I. Models and their applicability. J. Hydrol. 57, 207–231.
740 DOI:10.1016/0022-1694(82)90147-0.
741
742 Małoszewski, P., Rauert, W., Stichler, W., Herrmann, A. (1983). Application of flow models in
743 an alpine catchment area using tritium and deuterium data. J. Hydrol., 66(1), 319-330.
744 DOI:10.1016/0022-1694(83)90193-2.
745

McGuire, K.J., DeWalle, D.R., Gburek, W.J. (2002). Evaluation of mean residence time in subsurface waters using oxygen-18 fluctuations during drought conditions in the mid-Appalachians. J.Hydrol., 261(1), 132-149. DOI:10.1016/S0022-1694(02)00006-9.

McGuire, K.J., McDonnell, J.J. (2006). A review and evaluation of catchment transit time modeling. J. Hydrol. 330 (3), 543–563. DOI:10.1016/j.jhydrol.2006.04.020.

Moreno, A., Bartolomé, M., Pérez, C., Sancho, C., Cacho, I., Stoll, H., Delgado-Huertas, A., Edwards, R.L., Cheng, H. (2015). Tracking the origin of $\delta^{18}O$ variability in speleothems: examples from the Ordesa and Monte Perdido National Park (NE Iberia). In: J.P. Galve, J.M. Azañón, J.V. Pérez Peña and P. Ruano (eds.). Una Visión Global del Cuaternario. El Hombre como Condicionante de Procesos Geológicos. Reunión Nacional de Cuaternario, Granada (España): 82-85.

Mook, W.G., De Vries, J.J. (2000). Volume I, Introduction: Theory methods review. Environmental Isotopes in the Hydrological Cycle—Principles and Applications. International Hydrological Programme (IHP-V), Technical Documents in Hydrology (IAEA/UNESCO) 39(1). http://www-naweb.iaea.org/napc/ih/IHS_publication.html.

Niinikoski, P.I., Hendriksson, N.M., Karhu, J.A. (2016). Using stable isotopes to resolve transit times and travel routes of river water: a case study from southern Finland. Isotopes Environ. and Health Stud., 8: 1-13, DOI: 10.1080/10256016.2015.1107553.

Parisi, S., Paternoster, M., Kohfahl, C., Pekdeger, A., Meyer, H. Hubberten, H.W., Spilotro, G., Mongelli, G. (2011). Groundwater recharge areas of a volcanic aquifer system inferred from

771 hydraulic, hydrogeochemical and stable isotope data: Mount Vulture, southern Italy. Hydrogeol.
772 J., 19(1), 133-153. DOI:10.1007/s10040-010-0619-8.
773
774 Paternoster, M., Liotta, M., Favara, R. (2008). Stable isotope ratios in meteoric recharge and
775 groundwater at Mt. Vulture volcano, southern Italy. J.Hydrol., 348(1), 87-97.
776 DOI:10.1016/j.jhydrol.2007.09.038.
777
778 Peel, M.C., Finlayson, B.L., McMahon, T.A. (2007). Updated world map of the Köppen–Geiger
779 climate classification. Hydrol. Earth Syst. Sci.: 11: 1633–44. DOI: 10.5194/hess-11-1633-2007.
780
781 Poage, M.A., Chamberlain, C.P. (2001). Empirical relationships between elevation and the stable
782 isotope composition of precipitation and surface waters: considerations for studies of
783 paleoelevation change. Am. J. Science, 301(1): 1-15. DOI:10.2475/ajs.301.1.1.
784
785 Polo, E. (2015). Uso y manejo de nuevas tecnologías y herramientas SIG a partir de datos
786 hidrogeológicos en el Parque Nacional de Ordesa y Monte Perdido. Unpublished Master's
787 Thesis. Department of Geography and Regional Planning. University of Zaragoza.
788
789 Reddy, M.M., Schuster, P., Kendall, C., Reddy, M.B. (2006). Characterization of surface and
790 ground water $\delta^{18}O$ seasonal variation and its use for estimating groundwater residence times.
791 Hydrolog. Processes, 20(8): 1753-1772. DOI:10.1002/hyp.5953.
792
793 Ríos-Aragüés, L.M. (2003). Introducción al mapa geológico del Parque Nacional de Ordesa y
794 Monte Perdido. Sociedad Española de Espeleología y Ciencias del Karst (SEDECK), Boletín 5:
795 84–99.

Rowley, D.B., Pierrehumbert, R.T., Currie, B.S. (2001). A new approach to stable isotope-based paleoaltimetry: implications for paleoaltimetry and paleohypsometry of the High Himalaya since the Late Miocene. Earth and Planetary Science Letters, 188(1): 253-268. DOI:10.1016/S0012-821X(01)00324-7.

Rozanski, K., Araguás-Araguás, L., Gonfiantini, R. (1993). Isotopic patterns in modern global precipitation. In: PK Swart, KC Lohmann, J McKenzie, S Savin (eds.), Climate Change in Continental Isotopic Records. Am. Geophys. Union, Washington DC: 1-36.

Sapriza-Azuri, G., Jódar, J., Carrera, J., Gupta, H.V. (2013). Stochastic simulation of nonstationary rainfall fields, accounting for seasonality and atmospheric circulation pattern evolution. Math. Geosci. ,45(5): 621–645. DOI:10.1007/s11004-013-9467-0.

Sapriza-Azuri, G., Jódar, J., Navarro, V., Slooten, L.J., Carrera, J., Gupta, H.V. (2015). Impacts of rainfall spatial variability on hydrogeological response. Water Resour. Res., 51(2): 1300-1314. DOI:10.1002/2014WR016168.

Seguret, M. (1972): Étude tectonique des nappes et séries décollées de la partie centrale du versant sud des Pyrénées. Pub. USTELA, Ser. Geol. Struct. n.2, Montpellier.

Stewart, M.K., McDonnell, J.J. (1991). Modeling base flow soil water residence times from deuterium concentrations. Water Resour. Res. 27 (10), 2681–2693. DOI: 10.1029/91WR01569.

820 Stichler, W., Schotterer, U., Fröhlich, K., Ginot, P., Kull, C., Gäggeler, H., Pouyaud, B. (2001).
821 Influence of sublimation on stable isotope records recovered from high-altitude glaciers in the
822 tropical Andes. J. Geophys. Res., 106(D19): 22613–22620.
823
824 Stumpp, C., Małoszewski, P., Stichler, W., Fank, J. (2009). Environmental isotope ($\delta^{18}O$) and
825 hydrological data to assess water flow in unsaturated soils planted with different crops: case
826 study lysimeter station "Wagna" (Austria). J. Hydrol., 369(1): 198-208.
827 DOI:10.1016/j.jhydrol.2009.02.047.
828
829 Stumpp, C., Klaus, J., Stichler, W. (2014). Analysis of long-term stable isotopic composition in
830 German precipitation. J. Hydrol., 517: 351-361. DOI:10.1016/j.jhydrol.2014.05.034.
831
832 Vallejos, A., Díaz-Puga, M.A., Sola, F., Daniele, L., Pulido-Bosch, A. (2015). Using ion and
833 isotope characterization to delimitate a hydrogeological macrosystem. Sierra de Gádor (SE,
834 Spain). J. Geochem. Exploration, 155: 14-25. DOI:10.1016/j.gexplo.2015.03.006.
835
836 Yurtsever, Y., Gat, J.R. (1981). Atmospheric waters. Stable Isotope Hydrology: Deuterium and
837 Oxygen-18 in the Water Cycle. Vienna: IAEA: 103-142.
838
839 Zuber, A. (1986). Mathematical models for the interpretation of environmental radioisotopes in
840 groundwater systems. In: P Fritz & JC Fontes (eds.), Handbook of Environmental Isotope
841 Geochemistry, vol. 2, Terrestrial Environment B, Elsevier: Amsterdam: 1–59.
842

Tables

Table 1: Meteorological stations and springs sampled in the PNOMP (Lambán et al., 2015). The meteorological stations are sampled in a monthly base and the springs of the GW monitoring network are sampled quarterly.

Code	Type	Name	Lon (°)	Lat (°)	Z(m a.s.l.)	Periodical Sampling
P1	Met.St.	Fanlo-Góriz	0.016765	42.665154	2200	Yes
P2	Met.St.	Parador	-0.097628	42.657177	1216	Yes
P3	Met.St.	Fiscal	-0.112950	42.488675	772	Yes
2	Spring	Fuen de Tramasaguas	-0.082856	42.657661	1280	No
3	Spring	Fuen Caño	-0.078788	42.656719	1290	No
4	Spring	As Fuens	-0.064074	42.649752	1349	Yes
6A	Spring	Fuen Roya 1	-0.045506	42.651597	1348	Yes
6B	Spring	Fuen Roya 2	-0.044245	42.652465	1358	Yes
7	Spring	Fuen d´Arripas	-0.028227	42.639687	1440	No
8	Spring	Fuen as Gradas	-0.001739	42.639383	1700	No
9	Spring	Fuen Mochera	0.008249	42.644191	1807	Yes
10	Spring	Fuen l'Abellana	-0.045391	42.658933	1750	Yes
11	Spring	Fuen Cotatuero	-0.036008	42.662022	1800	No
12	Spring	Fuen De Soaso	0.014654	42.645481	1820	No
13	Spring	Fuen Carriata	-0.064759	42.662150	1820	No
14	Spring	Fuen de Soaso	0.007289	42.640965	1830	No
15	Spring	Fuen Gallinero	-0.056822	42.659443	1840	No
16	Spring	Fuen Freda	-0.030267	42.634247	1860	No
17	Spring	Fuen de L'Abe	-0.006619	42.634018	1920	No
18	Spring	Fuen Roldán	0.009466	42.665860	2136	Yes
19	Spring	Fuen de Goriz	0.016765	42.665154	2200	Yes
20	Spring	Fuen Fria	-0.001474	42.674584	2340	No
21	Spring	Collado Millares	-0.010544	42.676298	2420	No
22	Spring	Fuen dero Baño	0.105197	42.517707	689	Yes
23	Spring	Font Blanca	0.063073	42.644637	1710	Yes
24	Spring	Fuen dero Foratiello	0.059288	42.629142	1790	No
25	Spring	Fuen dero Furicon	0.015649	42.627445	2010	No
26	Spring	Fuen dero Esmoladera	0.006009	42.623503	2050	No
27	Spring	Fuen el Felcarral	0.066618	42.688439	1703	No
28	Spring	Fuen la Bispera	0.071265	42.690844	1930	No
29	Spring	Fuen de Escuaín	0.127760	42.604122	1050	Yes
42	Spring	Sucarraz	0.078970	42.686720	1468	Yes
43	Spring	Os Churros	0.082853	42.686751	1488	Yes
44	Spring	Esquinarasnos	0.070821	42.683572	1449	Yes

848 Table 2: Calibrated parameters from Eq. 2 applied to the seasonal isotopic water content in

849 rainfall samples in the meteorological stations.

Code	Z(m a.s.l)	$\overline{\delta^{18}O_{in}}$ (‰)	A_{in} (‰)
P1	2200	-11.25	4.97
P2	1216	-9.30	4.54
P3	780	-8.10	3.58

850

851

Table 3: Calibrated parameters from Eq. (1) applied to the seasonal isotopic GW content measured in the springs of the GW monitoring network. For each spring it is also provided the recharge zone elevation (Z_R) if a localized zone exists, the amplitude associated to that recharge zone (A_{Z_R}), the isotopic amplitude dampening factor (*f*), the estimated transit time by means of Exponential-Piston model (EPM), and the estimated EPM parameter (η).

	Z	$\overline{\delta^{18}O_{out}}$	A_{out}	Z_R	A_{Z_R}	f	τ	η	$1/\eta$
Code	(m a.s.l)	(‰)	(‰)	(m a.s.l.)	(m a.s.l.)	(-)	(yr)	(-)	(-)
9	1807	-12.20	1.80	2632	5.36	0.34	1.37	3.15	0.32
10	1750	-12.00	1.70	2541	5.28	0.32	1.60	2.99	0.33
23	1710	-11.80	2.00	2451	5.20	0.38	1.33	3.47	0.29
18	2136	-11.80	2.78	2450	5.20	0.53	1.12	4.47	0.22
4	1349	-11.80	1.00	2450	5.20	0.19	1.70	2.12	0.47
19	2200	-11.60	2.70	2359	5.12	0.53	1.26	4.72	0.21
44	1449	-11.21	1.16	2184	4.96	0.23	1.80	2.79	0.36
29	1050	-11.20	1.16	2177	4.95	0.23	1.52	2.31	0.43
6A	1358	-11.07	0.22	2118	4.90	0.05	4.48	1.39	0.72
42	1468	-11.00	1.15	2086	4.87	0.24	1.89	2.86	0.35
43	1488	-10.90	1.28	2041	4.83	0.26	1.88	3.21	0.31
6B	1358	-10.70	0.97	1950	4.75	0.20	2.05	2.29	0.44
22	689	-9.60	0.54	1450	4.30	0.13	2.41	1.93	0.52

Table 4: Mixing groundwater proportions of local recharge GW1 and regional discharge GW2 to explain the measured mean isotopic content in GW discharging at site 22 in terms of the considered elevation recharge Z_R for site 22.

		GW_{22}		GW_1		GW_2		Mix proportions	
Case	Z_R (m a.s.l.)	$\overline{\delta^{18}O}$ (‰)	$\overline{\delta^{2}H}$ (‰)	$\overline{\delta^{18}O}$ (‰)	$\overline{\delta^{2}H}$ (‰)	$\overline{\delta^{18}O}$ (‰)	$\overline{\delta^{2}H}$ (‰)	GW_1 (1-χ)	GW_2 χ
$Z_{R_{Max}}$	2632	-9.60	-67.73	-10.70	-69.04	-6.80	-64.38	72%	28%
$Z_{R_{Min}}$	1950	-9.60	-67.73	-12.20	-76.57	-5.45	-53.61	61%	39%

Table 5: Estimated chloride concentration in GW_2 by taking into account chloride concentrations in GW_1 and GW_{22} of 0.87 and 568 mg/L, respectively, and the GW mix proportions given in Table 4.

Case	χ [a]	C_{GW_2}(mg/L)
$Z_{R_{Max}}$	28%	2348
$Z_{R_{Min}}$	39%	1686

a: proportion of GW_2 in GW_{22} as expressed in Eq.13 and 14

Figures captions

Figure 1: Location map of the Ordesa and Monte Perdido National Park in central north-esatern Spain. Squares correspond to meteorological stations and circles to springs. The periodically sampled springs included in the GW monitoring network of the PNOMP are marked in red. The codes correspond to those in Table 1.

Figure 2: Geological map of PMOMP (modified from Lambán et al., 2015) and geological cross sections A-B and C-D (modified from Seguret (1972) and IGME-OAPN (2013)). Circles in red indicate the springs sampled periodically. The codes correspond to those in Table 1.

Figure 3: (A) Modified Stiff diagrams for the sampled springs in the PNOMP; in red the periodically sampled springs. (B) Average field T (solid circle) and EC (empty circle) for the periodically sampled springs in the PNOMP. Whiskers correspond to the measurement standard deviation. The code numbers correspond to those in Table 1.

Figure 4: Measured (open symbol) and seasonally averaged values (solid symbol) of $\delta^{18}O$ and $\delta^{2}H$ of (A) rainfall and (B) spring water, plotted in a δ dispersion diagram. The Global Meteoric Water Line (GMWL) and the Local Meteoric Water Line (LMWL), of slope 8 and respective deuterium excess of +10 and +18‰ are shown. Spring water tends to approach autumn precipitation with a contribution of winter precipitation.

Figure 5: Observed (circles) and fitted (line) isotopic $\delta^{18}O$ content in water from the meteorological stations (MSs) and springs (Sites) sampled periodically in the PNOMP. The identification codes correspond to those in Table 1.

Figure 6: Schematic representation of the GW system response $\delta_{out}(t,\tau)$ to a hypothetic input tracer function $\delta_{in}(t)$.

Figure 7: Amplitude of the output tracer function in terms the aquifer mean transit time for a fixed input tracer amplitude of 1‰ and different parameter values of the two LPM considered.

Figure 8: (A) Local isotopic altitudinal line $Z(\bar{\delta})$ obtained for a synthetic set of three meteorological stations. (B) Recharge is assumed to occur only in a certain zone of the vertical transect and therefore recharge elevation Z_R associated to a hypothetical spring obtained through $Z(\bar{\delta})$. (C) Isotopic amplitude altitudinal line $A(Z)$ associated to the synthetic meteorological stations set. (D) Amplitude of recharge A_{Z_R} associated to the recharge elevation Z_R obtained through $A(Z)$.

Figure 9: (A) Relationship between $\delta^{18}O$ and elevation and (B) Relationship between $A_{\delta^{18}O}$ and elevation, obtained for rainfall (solid symbol) and GW (empty symbol).

Figure 10: (A) Relationship between f and τ. (B) Relationship between $1/\eta$ and τ. Numbers correspond to those in Table 1.

Figure 11: (A) Rainfall infiltration capacity (RIC) in the PMOMP. Circles indicate springs; in red those periodically sampled. The codes correspond to those in Table 1. (B) Relationship between elevation and the mean RIC averaged by elevation intervals of 100 m. The shaded area at each side of the mean value corresponds to the standard deviation of RIC for the elevation interval (taken from Polo, 2015).

Figure-01

Click here to download Figure: Figure_01.pptx

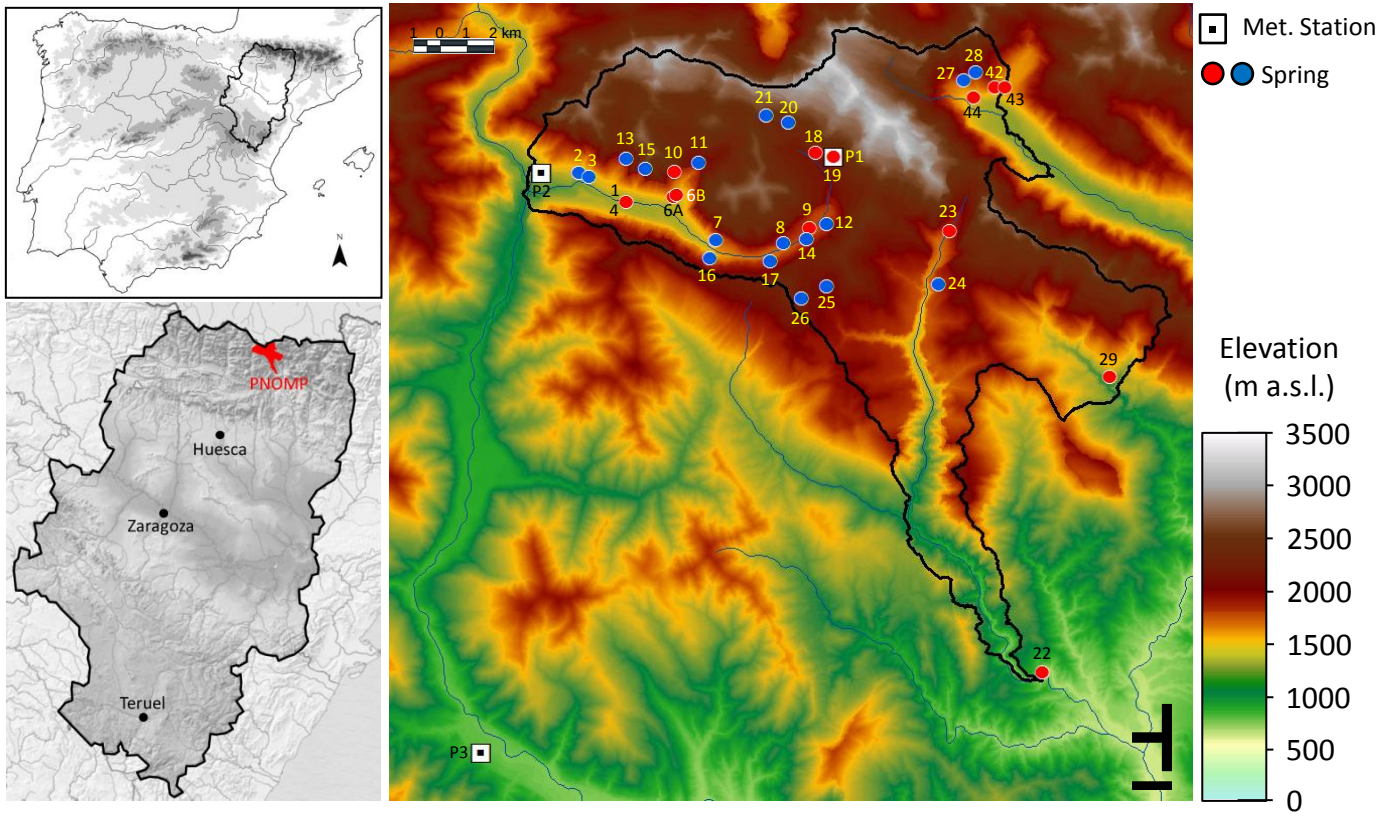

Figure-02

Click here to download Figure: Figure_02.pptx

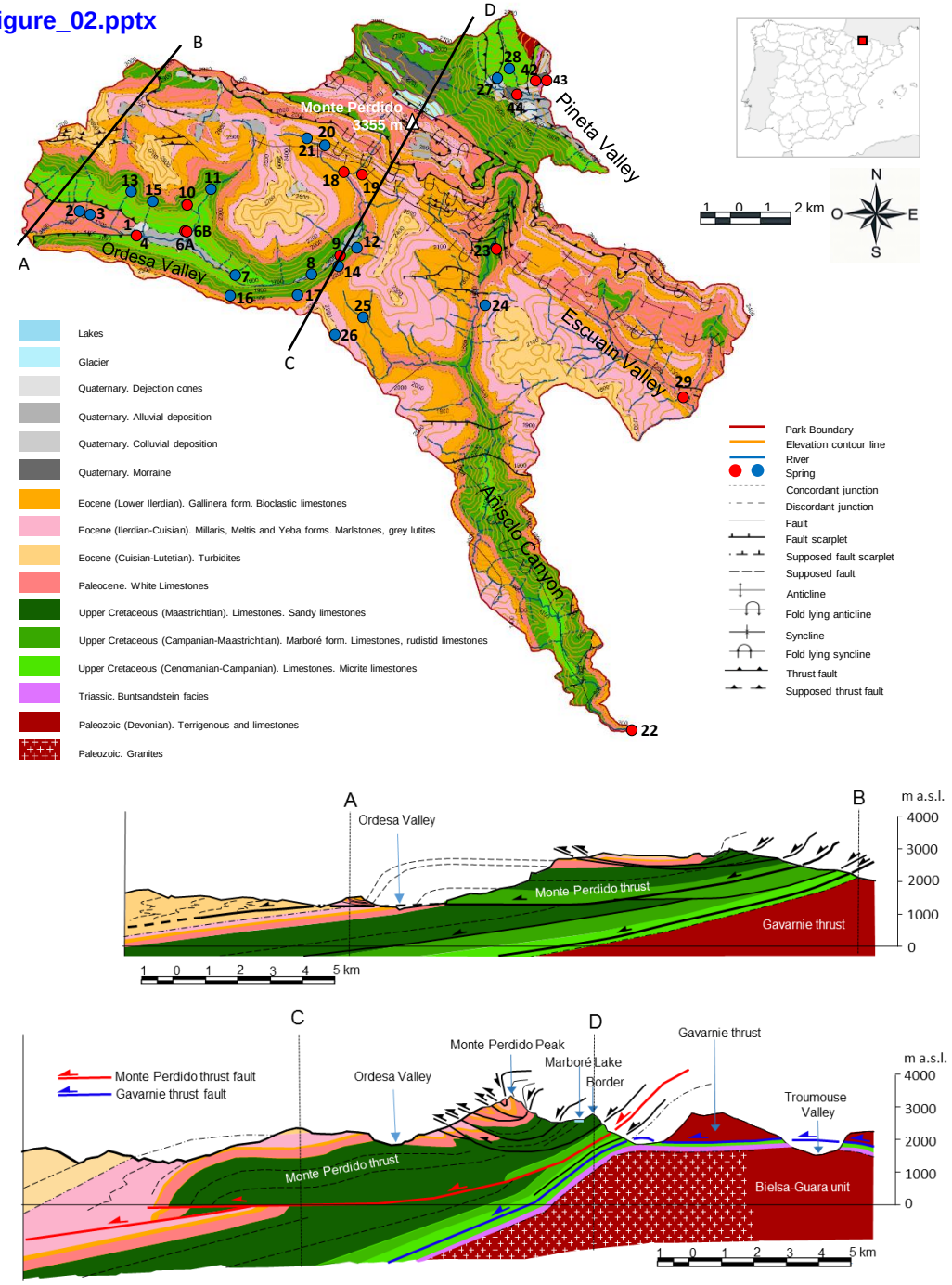

Figure-03

Click here to download Figure: Figure_03.pptx

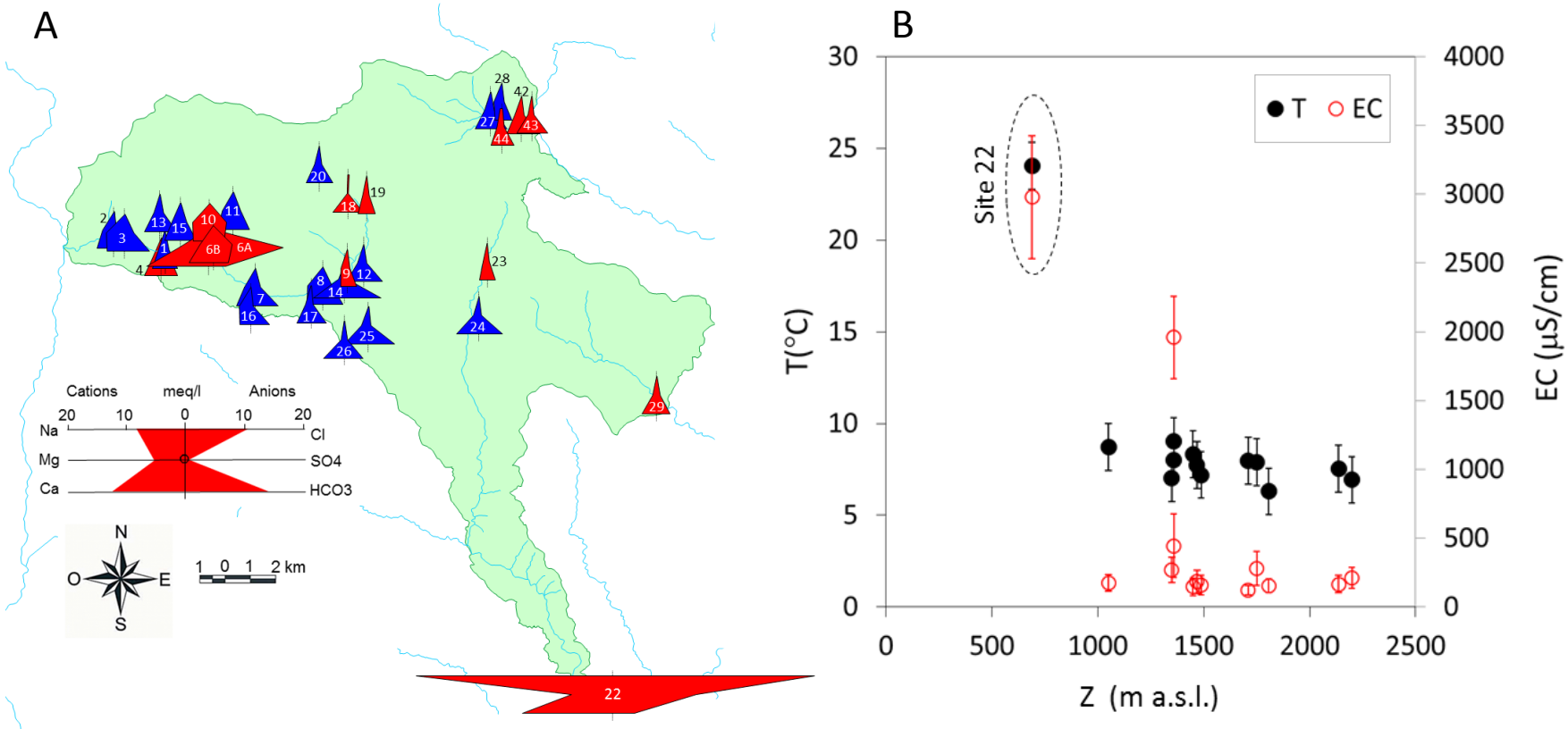

Figure-04

Click here to download Figure: Figure_04.pptx

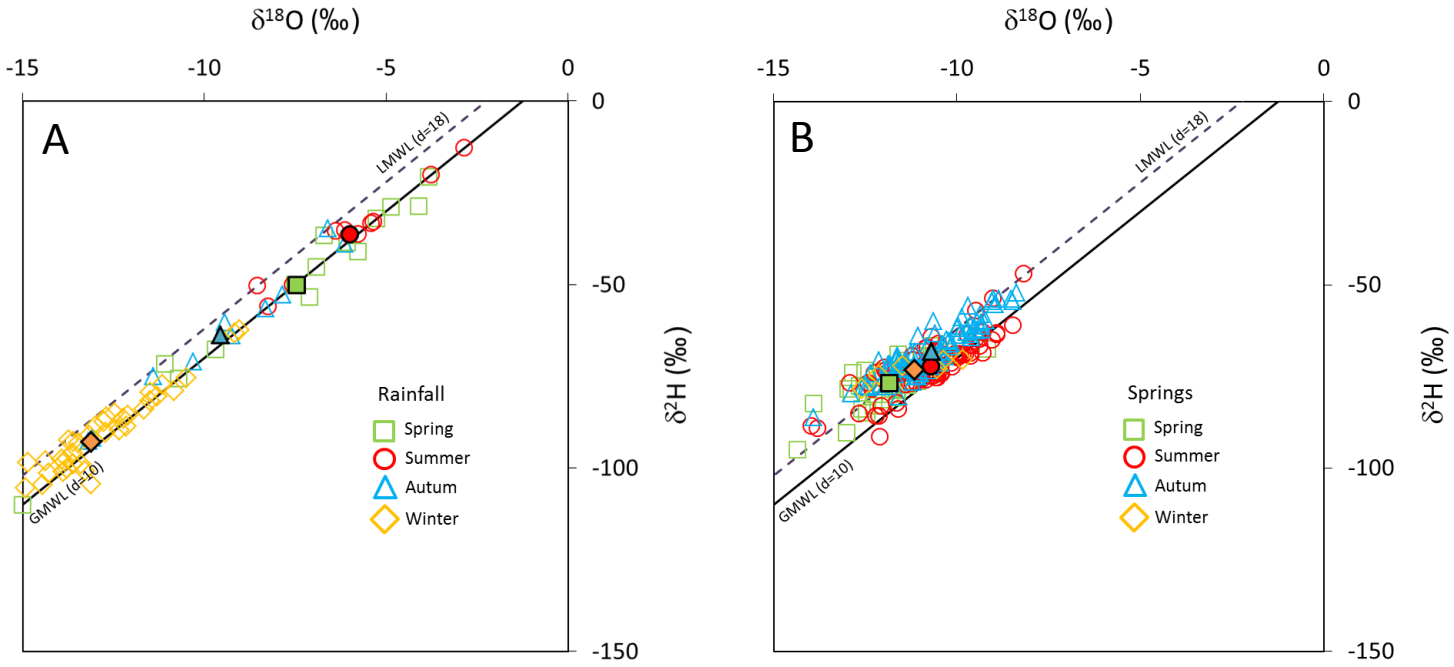

Figure-05

Click here to download Figure: Figure_05.pptx

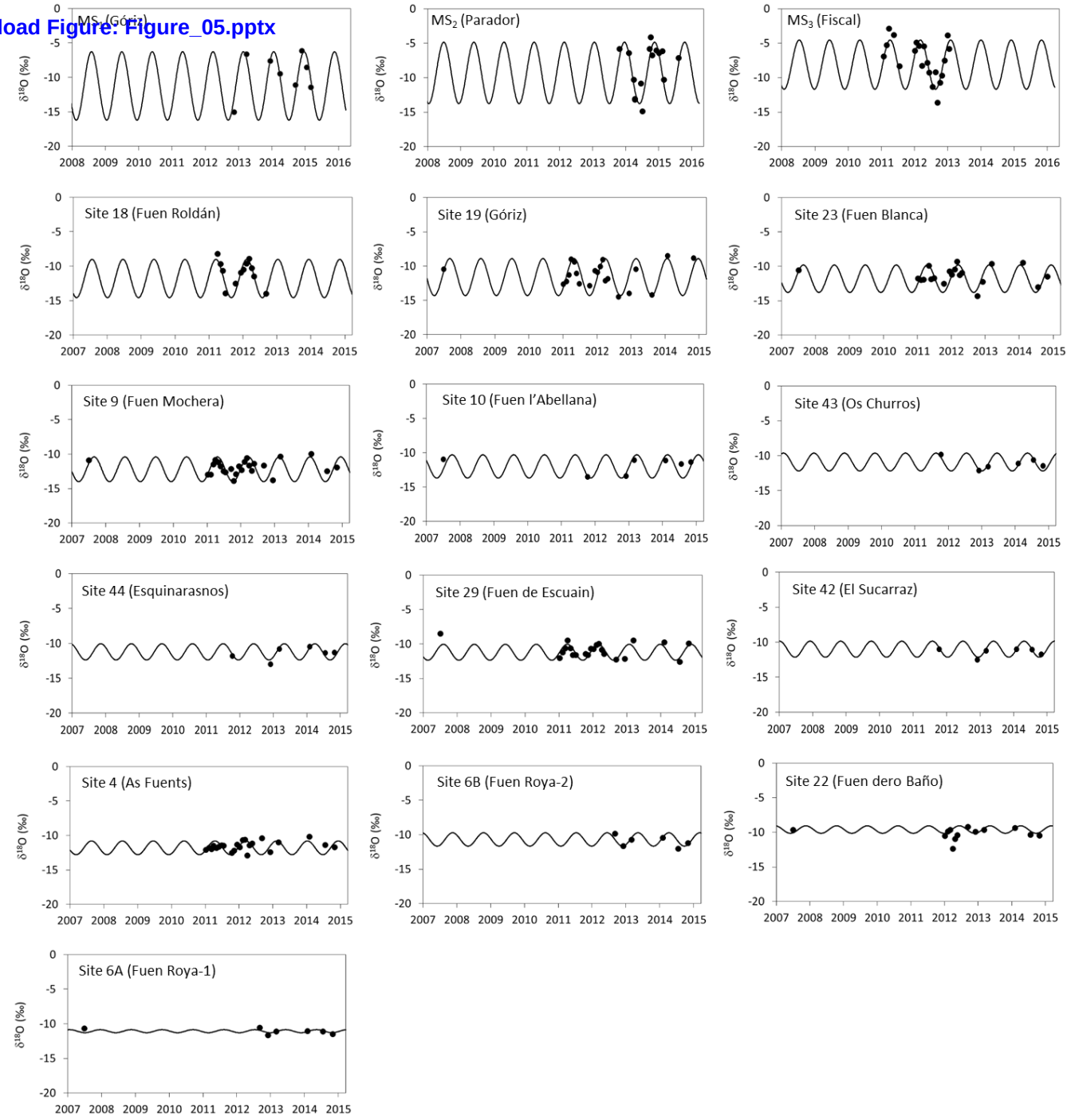

Figure-06

Click here to download Figure: Figure_06.pptx

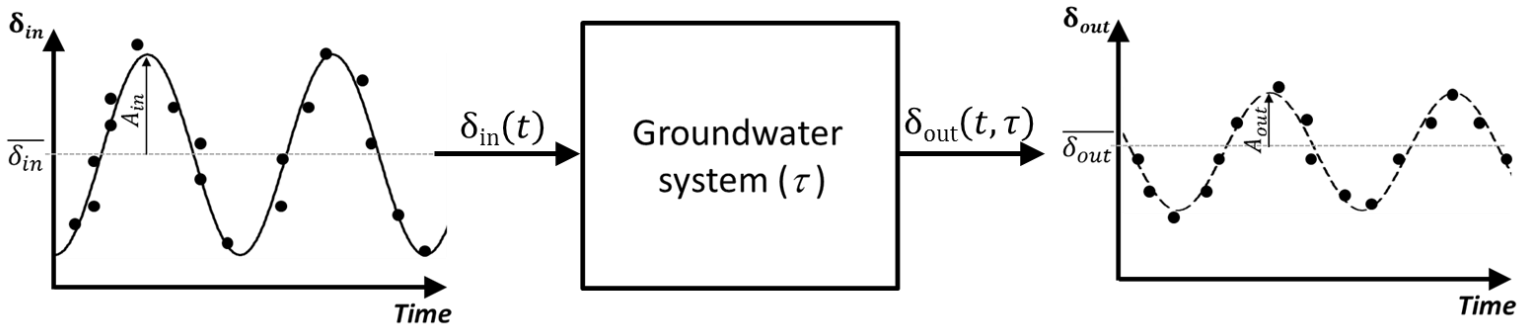

Figure-07

Click here to download Figure: Figure_07.pptx

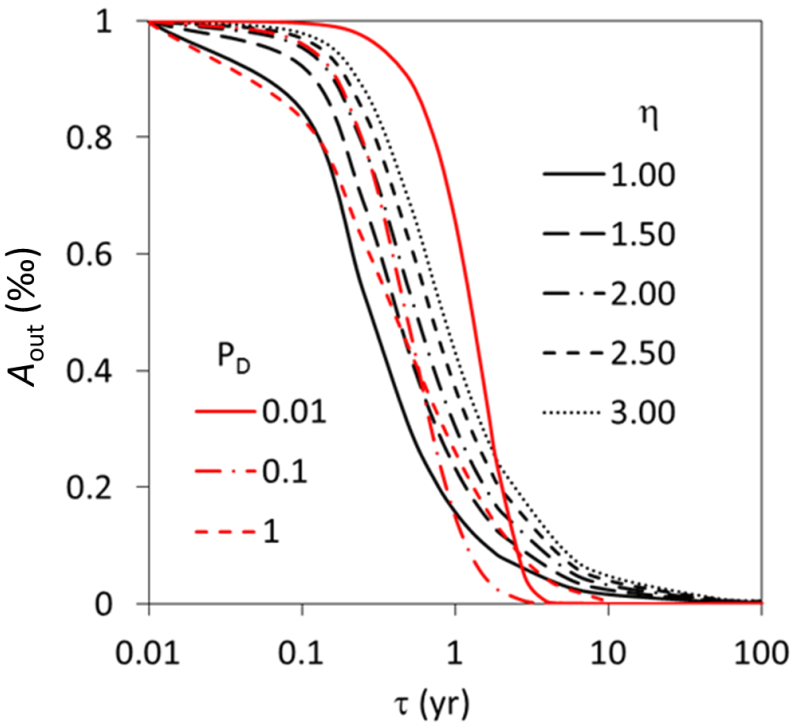

Figure-08

Click here to download Figure: Figure_08.pptx

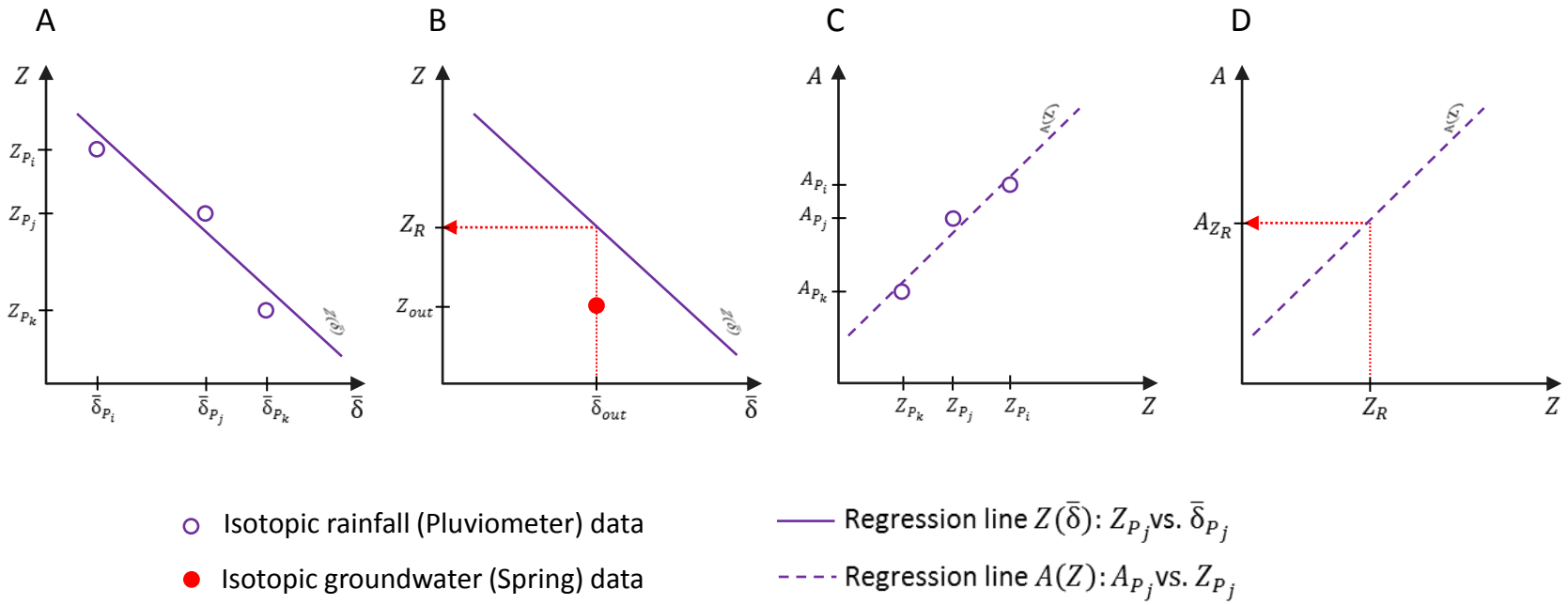

Figure-09

Click here to download Figure: Figure_09.pptx

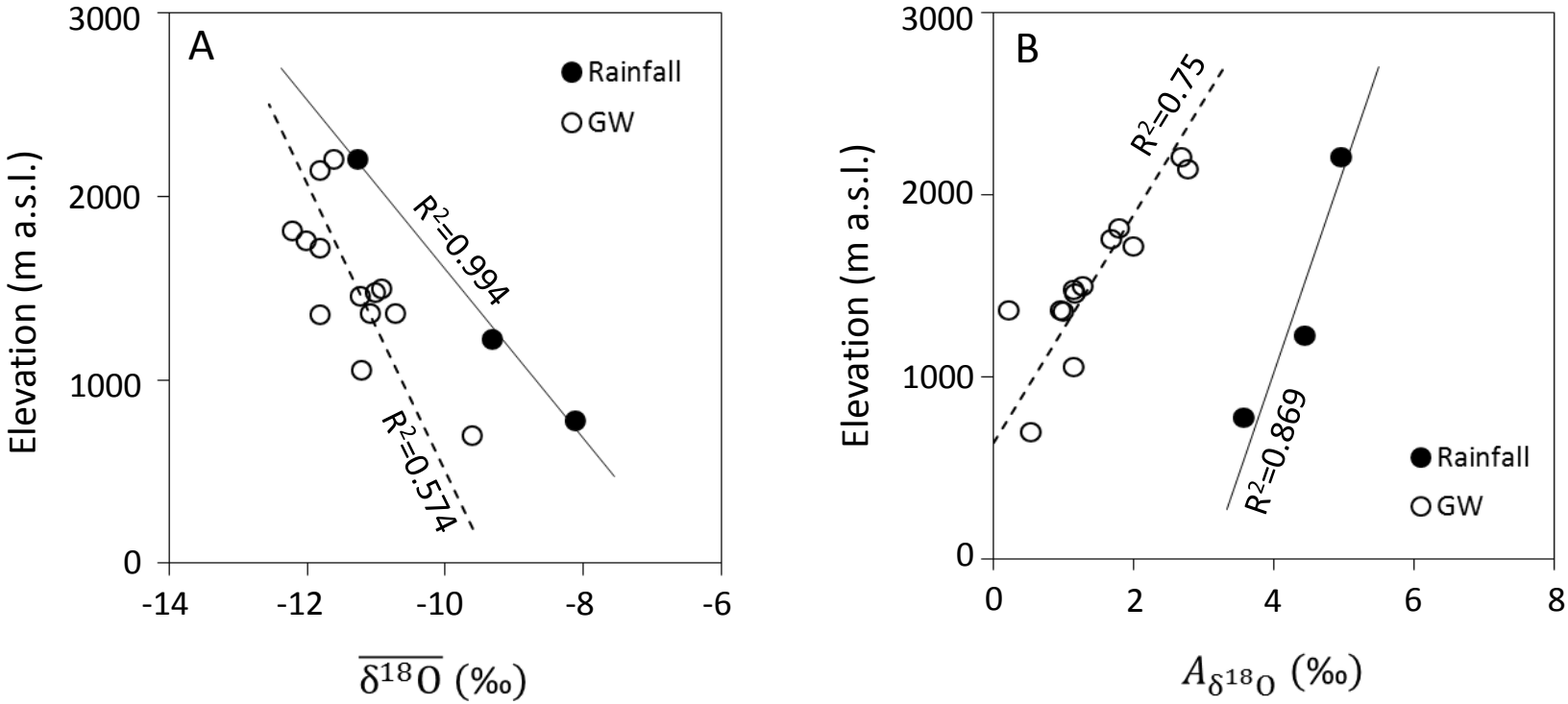

Figure-10

Click here to download Figure: Figure_10.pptx

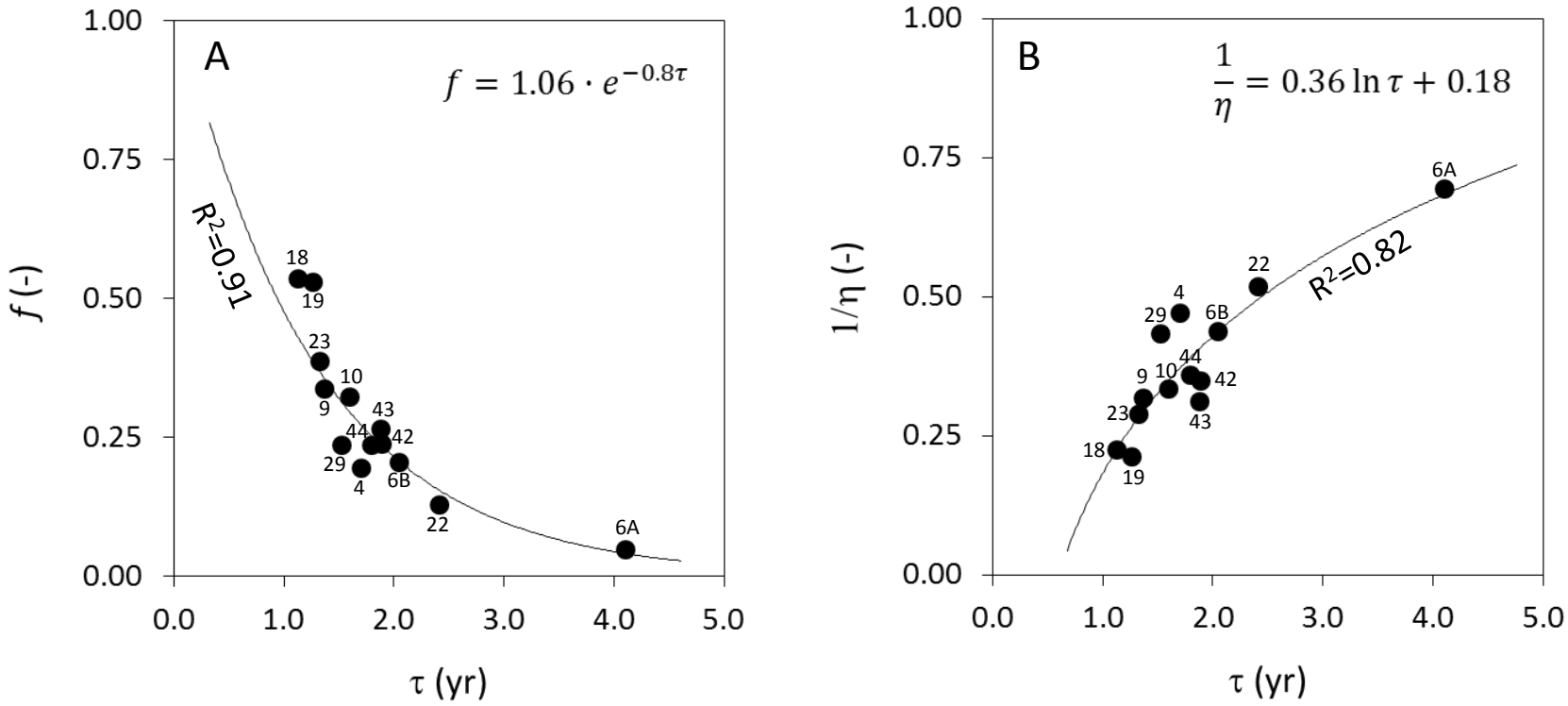

Figure-11

Click here to download Figure: Figure_11.pptx